nature communications

Article

https://doi.org/10.1038/s41467-024-53500-1

Regulation of minimal spindle midzone organization by mitotic kinases

Received: 20 February 2024

Accepted: 11 October 2024

Published online: 29 October 2024

Check for updates

Wei Ming Lim[1], Wei-Xiang Chew[1], Arianna Esposito Verza[2], Marion Pesenti[2], Andrea Musacchio[2,3,4] & Thomas Surrey[1,5,6]

During cell division, the microtubule cytoskeleton undergoes dramatic cell cycle-driven reorganizations of its architecture. Coordinated by changes in the phosphorylation patterns of a multitude of microtubule associated proteins, the mitotic spindle first self-assembles to capture the chromosomes and then reorganizes in anaphase as the chromosomes are segregated. A key protein for this reorganization is PRC1 which is differentially phosphorylated by the mitotic kinases CDK1 and PLK1. How the phosphorylation state of PRC1 orchestrates spindle reorganization is not understood mechanistically. Here, we reconstitute in vitro the transition between metaphase and anaphase-like microtubule architectures triggered by the changes in PRC1 phosphorylation. We find that whereas PLK1 regulates its own recruitment by PRC1, CDK1 controls the affinity of PRC1 for antiparallel microtubule binding. Dephosphorylation of CDK1-phosphorylated PRC1 is required and sufficient to trigger the reorganization of a minimal anaphase midzone in the presence of the midzone length controlling kinesin KIF4A. These results demonstrate how phosphorylation-controlled affinity changes regulate the architecture of active microtubule networks, providing new insight into the mechanistic underpinnings of the cell cycle-driven reorganization of the central spindle during mitosis.

As cells go through the cell cycle, the cytoskeleton undergoes several reorganizations to perform cell cycle state-specific functions. During cell division, the microtubule cytoskeleton initially assembles around chromosomes the mitotic spindle, a dynamic antiparallel microtubule array required to segregate the genetic material to the two daughter cells[1–3]. This structure persists until metaphase, but soon thereafter, as chromosomes are being moved towards the spindle poles in anaphase, a central spindle with increasingly shorter and more compacted antiparallel microtubule overlaps emerges, stabilizing the spindle center that contributes to determine the location of contractile ring formation for later cytokinesis.

This reorganization of the spindle architecture is ultimately a consequence of the decrease of CDK1 (cyclin dependent kinase 1) activity upon cyclin B degradation at the metaphase-to-anaphase transition[4–6]. As the balance between mitotic kinase and phosphatase activities changes during this transition, multiple proteins change their phosphorylation state causing midzone proteins to localize to, and reorganize, the antiparallel microtubule overlaps in the spindle center[7–10]. How changing phosphorylation patterns alter the activities of midzone proteins and how these changed biochemical properties then alter cytoskeleton architecture is mechanistically only poorly understood.

[1]Centre for Genomic Regulation (CRG), The Barcelona Institute of Science and Technology, Carrer del Dr. Aiguader 88, Barcelona, Spain. [2]Department of Mechanistic Cell Biology, Max Planck Institute of Molecular Physiology, Dortmund, Germany. [3]Max Planck School Matter to Life, Heidelberg, Germany. [4]Centre for Medical Biotechnology, Faculty of Biology, University Duisburg-Essen, Essen, Germany. [5]Universitat Pompeu Fabra (UPF), Barcelona, Spain. [6]Catalan Institution for Research and Advanced Studies (ICREA), Passeig de Lluis Companys 23, Barcelona, Spain. e-mail: thomas.surrey@crg.eu

https://doi.org/10.1038/s41467-024-53500-1

A critically important protein for midzone organization is PRC1 (protein regulator of cytokinesis 1)[11–14]. It localizes to spindles from yeast to humans, weakly in metaphase, and more strongly in anaphase[15–19]. It is a major protein interaction hub recruiting several other proteins to the spindle midzone in anaphase[3,12,17,20–22]. The dimeric PRC1 molecule selectively crosslinks antiparallel microtubules via its two spectrin domains[23–25]. These are flanked by positively charged, unstructured regions that enhance the microtubule binding affinity[25]. Interestingly, several phosphorylation sites for the mitotic kinases CDK1 and PLK1 (Polo-like kinase 1) are located in this unstructured region of PRC1 (Fig. 1A)[11,13,26,27].

The degree of phosphorylation of the CDK1 sites of PRC1 decreases as cells transition from metaphase to anaphase, concomitant with increased accumulation of PRC1 in the central spindle together with other midzone proteins[27,28]. At the same time the microtubule and PRC1 turnover decreases in the central spindle generating an increasingly compact assembly[15,19,29]. This suggests that dephosphorylation of the CDK1 sites on PRC1 may be needed for enhanced antiparallel microtubule binding of PRC1 and/or enhanced recruitment of other midzone proteins that can contribute to reorganize the central spindle. PLK1 phosphorylates PRC1 after the metaphase to anaphase transition and has been proposed to create its own docking site on PRC1 for later PLK1 functions required for correct cytokinesis[7,9,27]. However, one study reported that PLK1 already phosphorylates PRC1 in metaphase in order to prevent premature midzone formation[30]. In any case, phosphorylation of PRC1 by these two kinases appears to have very different biological functions, with the underlying biochemical logic still being poorly understood.

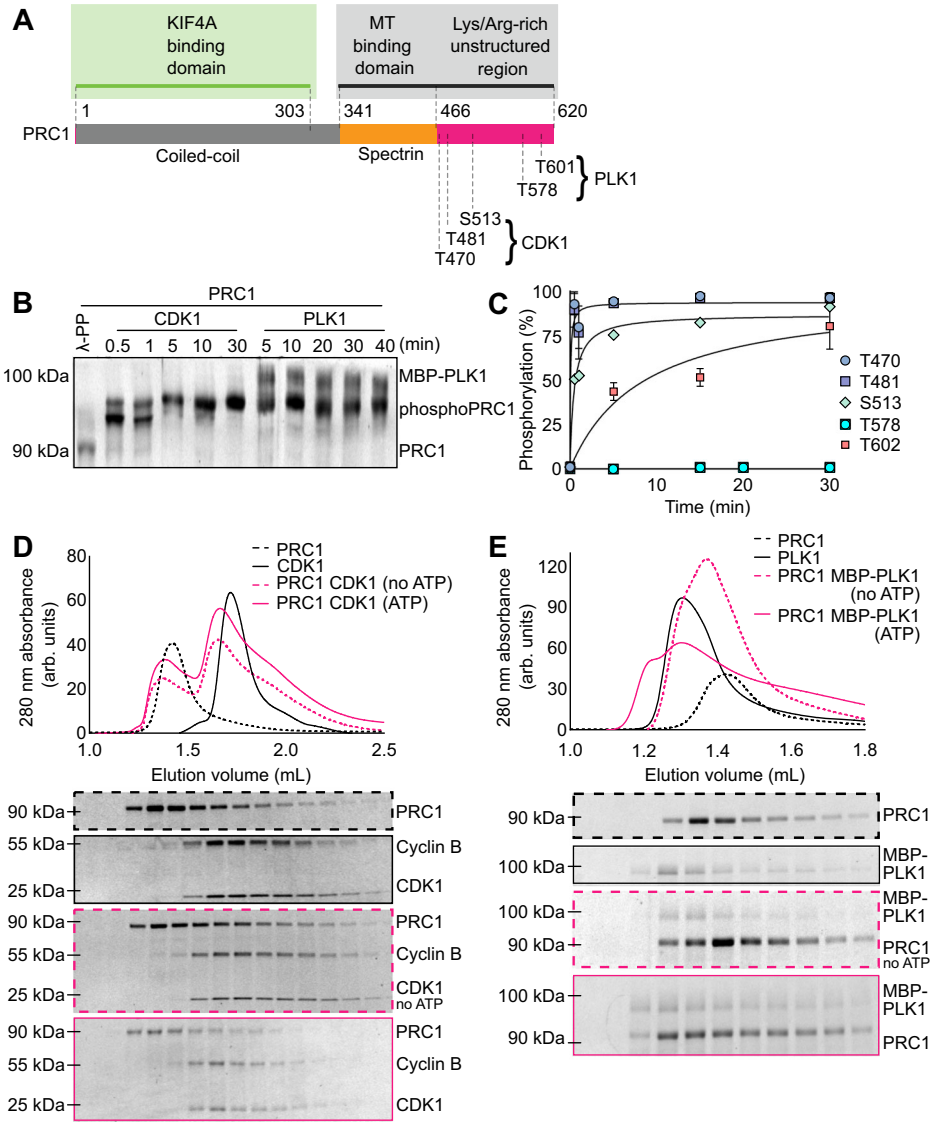

Fig. 1 | Phosphorylation of PRC1 by CDK1 and PLK1. A Schematic of the PRC1 sequence with domains and phosphorylation sites indicated, amino acid numbers refer to PRC1 isoform 2 which is used in all experiments. **B** Phos-tag gel of 5 μM PRC1-SNAP phosphorylated by 170 nM CDK1/cyclin B/CKS1 or 1 μM MBP-PLK1 for the indicated times, or incubated with 5 μM lambda protein phosphatase (λ-PP) for 30 min as negative control. $n = 5$ independent experiments. **C** Mass spectroscopic quantification of the degree of phosphorylation of PRC1 residues threonine 470, 481 and serine 513 (T470, T481, S513) by 170 nM CDK1/cyclin B/CKS1 and of PRC1 residues threonine 578 and 602 (T578, T602) by 1 μM MBP-PLK1 as a function of time. Data are presented as mean and errors bars are standard deviation. Lines are hyperbolic fits. $n = 5$ independent experiments for residues T470, T481, T578 and T602, and $n = 2$ independent experiments for residue S513. **D**, **E** Analytical size exclusion chromatography: Coomassie-stained SDS gels of PRC1 and kinases eluted from a gel filtration column at the indicated volumes. **D** 5 μM PRC1-SNAP or 5 μM CDK1/cyclin B/CKS1 or both mixed together in the presence of ATP were separated. **E** 5 μM PRC1 or 5 μM MBP-PLK1 or both mixed together either in the presence or absence of ATP, as indicated, were separated. The shift of a fraction of PRC1 and MBP-PLK1 in the presence of ATP to a smaller elution volume indicates binding of PLK1-phosphorylated PRC1 to MBP-PLK1. For D and E, $n = 3$ independent experiments. Source data are provided as a Source Data file.

The kinesin-4 KIF4A is one of the proteins that is recruited by PRC1 to the central spindle in anaphase[12,14,22]. The N-terminal dimerization domain of PRC1 binds the C-terminal part of KIF4A[12,31]. KIF4A is a plus-end directed motor protein that inhibits microtubule growth when it accumulates at microtubule plus ends[23,32] which is important for the length control of antiparallel microtubule overlaps in the spindle midzone[12,14,33].

In vitro reconstitutions with purified proteins can identify the minimal sets of activities that are required and sufficient for the self-organization of basic spindle sub-assemblies, such as microtubule asters mimicking spindle poles[34,35] or nematic networks mimicking the metaphase spindle center[36,37]. Previously, PRC1 and KIF4A were shown to be sufficient to self-organize antiparallel microtubule bundles with compact midzone-like microtubule overlaps mimicking the central part of anaphase spindles[23,38–40].

When purified PRC1 and KIF4A are combined with nucleating microtubules, PRC1 forms mixed polarity microtubule bundles and recruits KIF4A which in turn stops microtubule plus end growth once sufficient KIF4A has accumulated[23,31,32]. Moreover, KIF4A when bound to PRC1 can slide antiparallel microtubules, slowly compacting antiparallel microtubule overlaps[38]. This causes PRC1 and KIF4A to become concentrated in central overlaps with defined length from which parallel microtubule minus segments point outward, an architecture that is similar to central microtubule overlaps in the anaphase midzone.

The control of the transitions between different self-organized microtubule networks by kinases and phosphatases, as observed in cells, has however not been reconstituted in vitro yet. How the phosphorylation state of PRC1 affects its interaction with antiparallel microtubules and consequently its ability to cooperate with KIF4A to drive the self-organization of minimal midzones has not been investigated in vitro. It remains therefore unknown whether changing the PRC1 phosphorylation state is sufficient to control the reorganization from a metaphase to an anaphase microtubule architecture.

Here we perform fluorescence microscopy-based in vitro reconstitution experiments and demonstrate that phosphorylation of PRC1 by CDK1 strongly decreases its binding affinity for antiparallel microtubule overlaps. In contrast, phosphorylation by PLK1 does not affect this affinity, but causes recruitment of PLK1 to antiparallel microtubules. We show that CDK1 phosphorylation sites in PRC1 need to be dephosphorylated to organize microtubules into stable minimal midzones together with KIF4A. We then reconstitute phosphorylation-regulated transitions between metaphase and anaphase-like microtubule architectures in vitro. These experiments demonstrate that changing PRC1 phosphorylation is sufficient to reorganize active microtubule networks, providing new insight into the importance of controlling this interaction hub for metaphase-to-anaphase spindle reorganization in cells.

Results

Phosphorylation of PRC1 by CDK1 & PLK1

To study the effects of phosphorylation of PRC1 by the mitotic kinases CDK1 and PLK1 on the biochemical properties of PRC1, we purified human full-length PRC1 splice isoform 2 which was demonstrated to be the biologically active isoform during mitosis[27]. We also purified a ternary complex consisting of human CDK1/cyclin B/CKS1 that was shown previously to display high kinase activity[41] and active human PLK1. We were especially interested in the reported physiologically relevant phosphorylation sites situated in the C-terminal unstructured and positively charged part of PRC1 that is known to enhance binding of the neighboring spectrin domain of PRC1 to microtubules[25] (Fig. 1A).

The time course of phosphorylation of purified PRC1 by CDK1/cyclin B/CKS1 was monitored via gel-shift in a Phos-tag gel (Fig. 1B, left) and via Pro Q Diamond staining of a standard SDS gel (Suppl. Fig. 1A). PRC1 is unphosphorylated after purification (Suppl. Fig. 1B) and appeared to be fully phosphorylated within 5 min by 170 nM of the CDK1 complex, given that the degree of phosphorylation appeared to reach saturation (Fig. 1B, left). PRC1 was also phosphorylated by PLK1, apparently reaching saturation after 10-20 min in the presence of 1 μM PLK1 (Fig. 1B, right, and Suppl. Fig. 1A).

To measure the specific phosphorylation kinetics of the previously reported phosphorylation sites of PRC1 in mitosis we turned to quantitative mass spectrometry. Residues threonine 470 (T470), threonine 481 (T481)[11,13] and serine 513 (S513)[26] were all phosphorylated by CDK1/cyclin B/CKS1 essentially to completion within 5 min (Fig. 1C, red triangles and squares), demonstrating that these CDK1 sites can be efficiently phosphorylated in vitro.

Threonine 602 (T602)[27] was efficiently phosphorylated by PLK1, albeit more slowly than the CDK1 sites by CDK1 (Fig. 1C, blue circles), with kinetics measured by mass spectrometry being in agreement with the gel-based assays. In contrast, threonine 578 (T578), another reported PLK1-dependent phosphorylation site in cells[27], was not phosphorylated in vitro (Fig. 1C, blue diamonds). Instead, serine 554 and serine 68 respectively reached phosphorylation levels up to 90% and 68% within 30 min (Suppl. Fig. 1C). Phosphorylation of serine 554 was previously detected also in cells, but not further studied[7], whereas serine 68 has to our knowledge so far not been reported to be phosphorylated in cells.

To test if phosphorylation of PRC1 by one kinase affects the ability of the other kinase to phosphorylate PRC1, we sequentially phosphorylated PRC1 with the two kinases, starting with either CDK1 or PLK1. Quantitative mass spectrometry analysis showed the same degree of phosphorylation, irrespective of the order of kinase addition (Suppl. Fig. 1D). This result indicates that CDK1 and PLK1 phosphorylate PRC1 independently of each other.

Next, we tested by size exclusion chromatography whether PRC1 interacts stably with these two kinases. No strong interaction between PRC1 and the CDK1 complex was detected in the presence of ATP to allow phosphorylation of PRC1 (Fig. 1D). Conversely, a considerable fraction of PLK1 formed a stable complex with PRC1, provided ATP was present to allow phosphorylation of PRC1 by PLK1 (Fig. 1E, Suppl. Fig. 1E).

In conclusion, CDK1 very efficiently phosphorylates T470, T481 and S513 of PRC1 in vitro without becoming stably bound to its substrate. The slower kinase PLK1 phosphorylates T602 of PRC1, resulting in stable binding of the kinase to its substrate, demonstrating that PLK1 can indeed 'self-prime' its binding to PRC1, as suggested previously based on studies in cells[27], and as also shown for another mitotic protein[42].

Effect of PRC1 phosphorylations by CDK1 and PLK1 on antiparallel microtubule binding

To study how phosphorylation of PRC1 by the two mitotic kinases affects its function, we pre-phosphorylated fluorescently labeled PRC1-Alexa546 with either one or the other kinase using conditions that ensured essentially complete phosphorylation. We then compared the binding of unphosphorylated and phosphorylated PRC1 to antiparallel microtubules in a TIRF microscopy-based in vitro assay in which pairs of dynamic Alexa647-labeled microtubules growing from surface-immobilized stabilized microtubule 'seeds' form antiparallel overlaps connected by PRC1, as described previously[23] (Fig. 2A, Supplementary Movie 1).

Increasing the concentration of unphosphorylated PRC1-Alexa546 led to increased binding of PRC1 to antiparallel microtubule overlaps and finally to saturation of binding (Fig. 2B, top, and Suppl. Fig. 2A top). The measured PRC1-Alexa546 fluorescence intensity plotted as a function of the PRC1 concentration indicated a dissociation constant of 10 nM (Fig. 2C, circles), in agreement with previous measurements for *Xenopus laevis* PRC1[23]. In contrast, CDK1-phosphorylated PRC1 bound much more weakly to microtubules (Fig. 2B bottom, Suppl. Fig. 2A bottom), not even reaching half-

https://doi.org/10.1038/s41467-024-53500-1

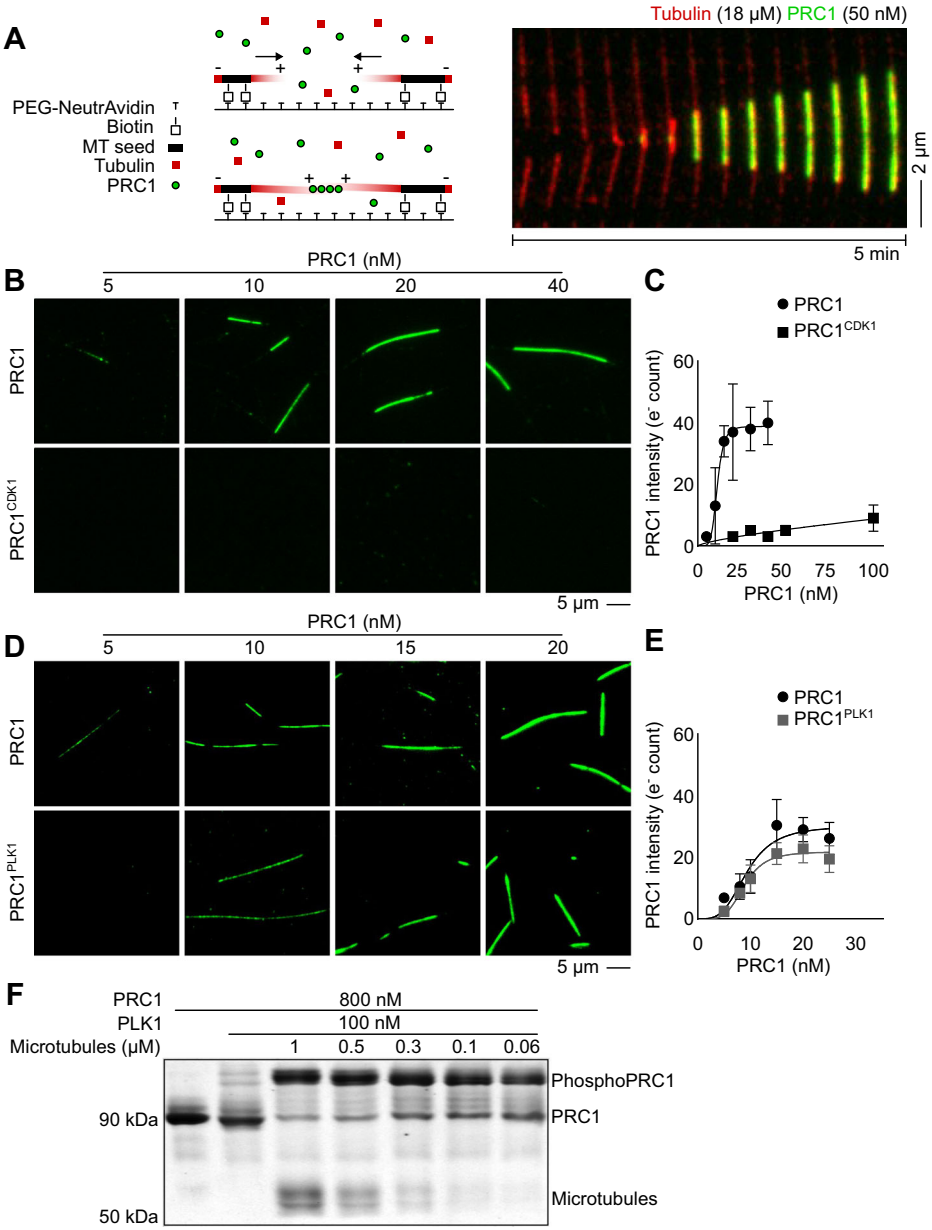

Fig. 2 | Phosphorylation of PRC1 by CDK1 reduces PRC1 binding to antiparallel microtubule overlaps, indirectly affecting phosphorylation by PLK1 in overlaps. A Schematic of the antiparallel microtubule pair assay (left) and an example time sequence of TIRF microscopy images of the formation of an antiparallel microtubule (red) overlap in the presence of PRC1 at the indicated concentrations. **B** TIRF microscopy images of unphosphorylated (top) or fully CDK1-phosphorylated (bottom) PRC1-Alexa546 binding to antiparallel overlaps of Alexa647-microtubules elongating from surface immobilized microtubule 'seeds'. Alexa647-tubulin concentration is 18 μM, PRC1 concentrations and scale bar as indicated. Same data displaying also the microtubule channel in Suppl. Figure 2A. **C** Quantification of the PRC1-Alexa546 fluorescence intensity measured in antiparallel microtubule overlaps for unphosphorylated and fully CDK1-phosphorylated PRC1 as a function of the PRC1 concentration. A Hill function fit to the data of unphosphorylated PRC1 yields a dissociation constant of 10 ± 0.75 nM. A linear regression is shown for the data of phosphorylated PRC1. Error bars are standard deviation. $n = 3$, total length of 100 μm antiparallel overlaps for each tested concentration. **D** TIRF microscopy images of unphosphorylated (top) or fully PLK1-phosphorylated (bottom) PRC1-Alexa546 binding to antiparallel overlaps of Alexa647-microtubules elongating from surface-immobilized microtubule 'seeds'. Alexa647-tubulin concentration is 18 μM, PRC1 concentrations and scale bar as indicated. Same data displaying also the microtubule channel are shown in Suppl. Figure 2B. **E** PRC1-Alexa546 fluorescence intensity in antiparallel microtubule overlaps for unphosphorylated and PLK1-phosphorylated PRC1 as a function of the PRC1 concentration. A Hill function fit to the data of unphosphorylated and PLK1-phosphorylated PRC1 yields dissociation constants of 9.3 ± 0.46 nM and 9.6 ± 0.68 nM. Error bars are standard deviation. $n = 3$ independent experiments, total length of 100 μm antiparallel overlaps for each tested concentration. Fluorescence intensity in (**C**) and (**E**) are converted to electron count. **F** Phos-tag gel of 800 nM PRC1-SNAP phosphorylated for 5 min by 100 nM PLK1 with or without stabilized microtubules at different (polymerized tubulin) concentrations, or unphosphorylated PRC1 as negative control. $n = 5$ independent experiments. Source data are provided as a Source Data file.

saturation of binding at 100 nM (Fig. 2C, squares, Supplementary Movie 2), demonstrating that phosphorylation by CDK1 decreases the affinity of PRC1 binding to antiparallel microtubules by more than a factor of 10 under these conditions.

In contrast, PLK1-phosphorylated PRC1 bound to antiparallel microtubule overlaps with essentially unchanged affinity compared to unphosphorylated PRC1 (Fig. 2D, Suppl. Fig. 2B), but with a slightly reduced density at saturation (Fig. 2E, Supplementary Movie 3). A likely

explanation for this reduced binding at saturation is steric hindrance by PLK1 that is recruited to antiparallel microtubule overlaps by PLK1-phosphorylated PRC1 (Suppl. Fig. 3A–E), in agreement with the notion that PLK1 creates its own docking site by phosphorylating PRC1 to be recruited to the spindle midzone in anaphase cells[27].

Next, we asked if the local accumulation of PLK1 in PRC1 containing antiparallel microtubule overlaps promotes PRC1 phosphorylation. After addition of PLK1 at a low concentration, we compared the degree of PRC1 phosphorylation in the absence and presence of increasing concentrations of stabilized microtubules. Whereas only a mild degree of phosphorylation was observed under these conditions without microtubules (Fig. 2F, lane 2, mild PRC1 band shift in a Phos-tag gel), addition of microtubules caused a remarkable increase of the degree of PRC1 phosphorylation by PLK1 (Fig. 2F, lanes 3 to 7, strong shifts of PRC1 gel bands). This result shows that PLK1 phosphorylates PRC1 between antiparallel microtubules to recruit itself to PRC1, thereby enhancing its local kinase activity.

The different effects that the two mitotic kinases have on the affinity of PRC1 binding to antiparallel microtubules can be explained by the positions of the respective phosphorylation sites within the positively charged unstructured C-terminal of PRC1 (Fig. 1A). The positive charge closer to the spectrin domain is expected to enhance binding of PRC1 to microtubules more strongly than charge at a larger distance. Consequently, a reduction of the net positive charge by phosphorylation of residues in the vicinity of the spectrin domain, where the CDK1 phosphorylation sites are located (Fig. 1A), is expected to weaken binding more efficiently than phosphorylation at a larger distance, where the PLK1 sites are. On the other hand, tethering PLK1 to the end of the unstructured PRC1 tail may be the optimal position for allowing it to access other substrates locally in the central spindle.

In conclusion, CDK1 selectively controls the binding affinity of PRC1 for antiparallel microtubules, whereas PLK1 has no effect on this affinity, but phosphorylates PRC1 in order to recruit itself to antiparallel overlaps, mainly to enhance its local concentration where it is needed to phosphorylate other mitotic substrates locally in anaphase.

Stable minimal PRC1/KIF4A midzones can only self-organize if PRC1 is not CDK1-phosphorylated

Next, we investigated how mitotic kinase-mediated phosphorylation of PRC1 affects its ability to generate anaphase-like mini-spindles together with KIF4A (Fig. 3A, scheme). We mixed unphosphorylated PRC1-Alexa546, KIF4A-mGFP and Alexa647-labeled tubulin in solution and allowed the nucleated microtubules to become organized by PRC1 and KIF4A. Antiparallel microtubule bundles self-assembled with microtubule plus-end overlaps at the center marked by accumulated PRC1 and KIF4A, and parallel microtubule minus segments extending out on both sides of the overlaps (Fig. 3B, top row, Supplementary Movie 4), as shown previously[38]. Under these conditions, KIF4A stops microtubule plus end growth[23,38], and increasing the KIF4A concentration leads to shorter, more compacted overlaps due to the KIF4A motors bound to PRC1, forcing all molecules in the overlap closer together by their antiparallel microtubule sliding activity (Fig. 3C, left), as characterized in detail previously[23,38].

When PLK1-phosphorylated PRC1 was used in these experiments, we did not observe an effect on minimal midzone bundle organization (Suppl. Fig. 3D), in agreement with PRC1's affinity for antiparallel microtubule binding not being altered by PLK1 phosphorylation. PLK1 was recruited to minimal midzones by PLK1-phosphorylated PRC1 (Suppl. Fig. 3D, E), as expected from our in vitro experiments with microtubule pairs (Fig. 2D, E) and recapitulating observations in cells[7,9,27]. Slightly less PLK1-phosphorylated PRC1 than unphosphorylated PRC1 accumulated in minimal midzone overlaps, again in agreement with the microtubule pair experiments and reminiscent of a report showing that PLK1 phosphorylation of PRC1 prevents excessive accumulation of PRC1 in anaphase midzones in cells[43].

In contrast, when CDK1-phosphorylated PRC1 was used in minimal midzone self-organization experiments instead of unphosphorylated PRC1, we observed in the lower KIF4A concentration regime very long microtubule bundles without any visible local accumulation of PRC1 or KIF4A, indicating that both proteins bind now all along unorganized mixed polarity bundles and that plus end microtubule growth is not stopped under these conditions, leading to an increased microtubule mass (Fig. 3B, bottom left, 3C, middle, Supplementary Movie 4). In separate experiments, we demonstrated by size exclusion chromatography experiments that phosphorylation of PRC1 by CDK1 does not affect its interaction with KIF4A (Suppl. Fig. 5A). Therefore, the different types of microtubule organization by phosphorylated PRC1 in the presence of KIF4A is a consequence of weaker PRC1 binding to microtubules, which in turn also leads to a weaker recruitment of KIF4A to microtubules, simply because phosphorylated PRC1 accumulates less on the microtubules, allowing microtubule plus ends to grow. This indirect effect on the recruitment of KIF4A can be demonstrated in so-called end-tag experiments under conditions where PRC1 is transported to the plus ends of individual microtubules by KIF4A, leading both proteins to accumulate there and stop plus end growth provided sufficient KIF4A is recruited (Suppl. Fig. 5B)[31]. Substantially higher concentrations of phosphorylated PRC1 than unphosphorylated PRC1 were required to stop plus-end growth, showing that less KIF4A binds when PRC1 binds the microtubule more weakly in its phosphorylated form (Suppl. Fig. 5B).

When higher concentrations of KIF4A were used in the anaphase mini-spindle self-organization experiment in the presence of CDK1-phosphorylated PRC1, microtubule bundles became polarity-sorted again, displaying regions of compacting antiparallel overlaps in which phosphorylated PRC1 and KIF4A accumulated (Fig. 3B - bottom right, Supplementary Movie 4). However, these antiparallel overlaps were not stable, as they frequently bent and occasionally broke (Fig. 3C, right). This shows that increasing the KIF4A concentration can partly compensate for reduced PRC1 binding to microtubules in its phosphorylated state, but phosphorylated PRC1 did not allow the maintenance of stable compacted antiparallel microtubule overlaps.

A wider examination of the parameter space of minimal midzone organization by varying not only the KIF4A but also the PRC1 concentration revealed that stable compacted antiparallel overlaps could not be formed with phosphorylated PRC1 under any of the tested conditions (Fig. 3D - bottom). Bundles were either disorganized, bent or broke apart after attempted minimal midzone formation. In stark contrast, in the presence of unphosphorylated PRC1, mini-midzones of compacted antiparallel microtubule overlaps formed stably over a wide range of KIF4A and PRC1 concentrations (Fig. 3D - top).

To investigate the molecular origin of mini-midzone instability caused by CDK1-phosphorylation of PRC1, we turned to Cytosim-based computer simulations using a variant of a previous one-dimensional model for minimal midzone formation (Suppl. Fig. 6A)[38]. We simulated small bundles consisting of four microtubules of constant length. To mimic the effect of phosphorylation by CDK1, we varied the PRC1 affinity for microtubule binding by varying its unbinding rate from microtubules. We observed that the lower the PRC1 affinity (i.e. the higher the unbinding rate) was, the shorter the microtubule overlaps became until they finally became unstable and broke apart (Suppl. Fig. 6B). Concomitantly the density of PRC1 in the overlaps was reduced (Suppl. Fig. 6C), as observed experimentally (Fig. 2B). The increasingly variable overlap length could be explained by an increasing variation of the relative microtubule sliding speeds with decreasing PRC1 affinity (Suppl. Fig. 6D). When microtubules in the bundle are connected to multiple antiparallel microtubules, and if these antiparallel pairs, taken in isolation, would slide with

https://doi.org/10.1038/s41467-024-53500-1

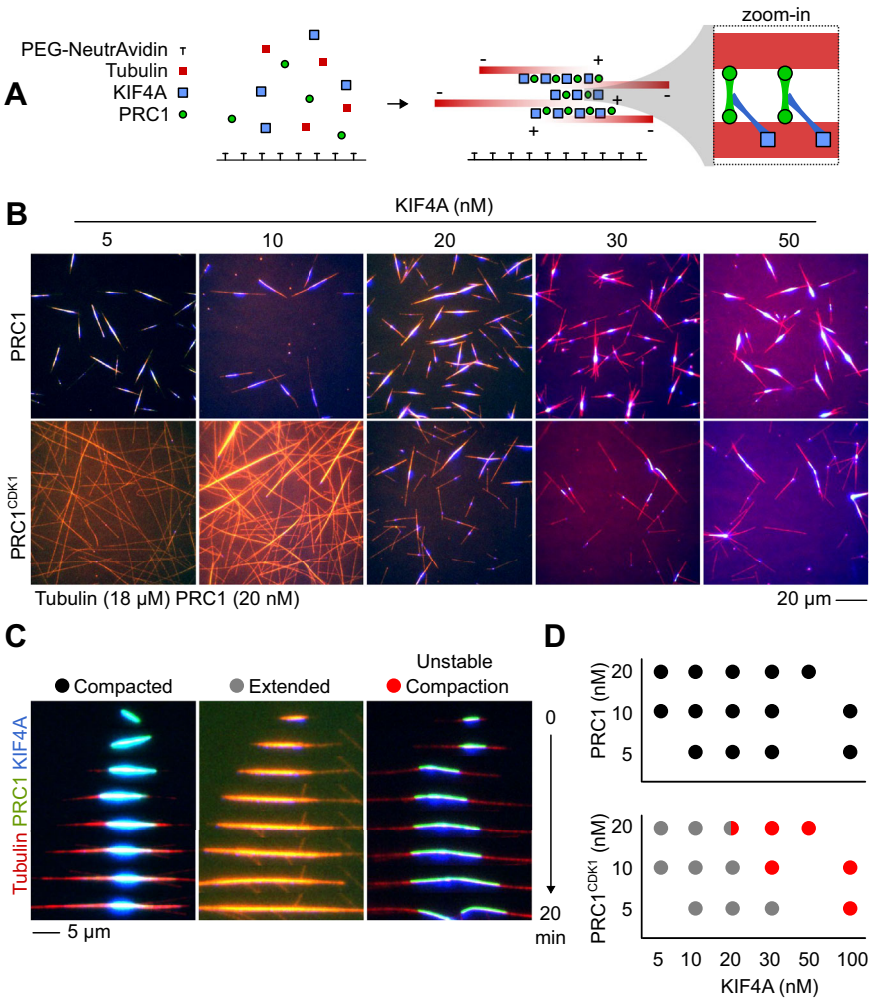

Fig. 3 | Phosphorylation of PRC1 by CDK1 prevents stable minimal midzone organization in the presence of KIF4A. A Schematic of the minimal midzone self-organization assay. Purified PRC1 and KIF4A organize microtubules into bundles with compacted antiparallel overlaps at the center. PRC1 crosslinks antiparallel microtubules and recruits KIF4A to the antiparallel overlap zone. In turn, KIF4A walks towards the microtubule plus-end pulling on PRC1, generating antiparallel microtubule sliding, which compacts the antiparallel overlap at the bundle center. Parallel microtubule minus segments grow outward, gnerating an organization similar to anaphase midzone bundles. **B** TIRF microscopy images taken ~20 min after self-organization of microtubule bundles in the presence of 20 nM unphosphorylated (top) or fully CDK1-phosphorylated (bottom) PRC1-Alexa546 (green), 5–50 nM KIF4A-mGFP (blue), and 18 μM Alexa647-tubulin (red). See Suppl. Figure 4 for same data displaying the individual channels separately. Scale bar as indicated. **C** Example TIRF microscopy images of a time series of (left) a bundle with a stable compacted antiparallel microtubule overlap (minimal midzone) in the presence of 20 nM unphosphorylated PRC1 and 30 nM KIF4A (left), a bundle that fails to form a compacted overlap in the presence of 20 nM CDK1-phosphorylated PRC1 and 10 nM KIF4A (middle), and an antiparallel bundle that first forms a compacted overlap that is then however unstable and bends in the presence of 20 nM CDK1-phosphorylated PRC1 and 30 nM KIF4A. The Alexa647-tubulin concentration was always 18 μM. Scale bar as indicated. **D** Phase spaces of antiparallel bundle self-organization for unphosphorylated and CDK1-phosphorylated PRC1. Each symbol represents a minimum of 3 individual experiments with 10–20 observed microtubule bundles per experiment, and a symbol with two colors represents a condition at the boundary between two regimes where the outcome of self-organization can lead to either one or the other type of organization. Symbols as in (**C**).

different speeds, the entire bundle may be expected to be under shearing forces that could lead microtubules to bend before breaking, as we observed experimentally (Fig. 3C, right). These simulations support the notion that the microtubule-binding affinity of PRC1 needs to be sufficiently high to allow stable anaphase-like midzone formation.

We conclude that the microtubule-binding affinity of unphosphorylated PRC1 allows stable and compacted midzone-like antiparallel microtubule overlaps to self-organize in the presence of KIF4A. Conversely, CDK1-phosphorylated PRC1 does not support this type of anaphase architecture. Hence phosphorylation of PRC1 by CDK1 appears to be sufficient to ensure that a critical aspect of anaphase microtubule organization cannot form prematurely in metaphase when CDK1 activity is high.

Transitions between metaphase and anaphase-like microtubule architectures induced by changes in the CDK1-phosphorylation state of PRC1

We next asked whether changing the CDK1-phosphorylation state of PRC1 will be sufficient to allow switching from one self-organized minimal microtubule network architecture to another architecture, mimicking cell cycle-driven microtubule cytoskeleton reorganizations in cells. This required the delivery of protein activities to a self-organizing microtubule system without inducing turbulence. We therefore developed a flow chamber that was connected via a 1 mm opening to a top reservoir (Fig. 4A) to which proteins could be added after some time of self-organization and from where these proteins could then diffuse into the observation chamber. We could show in test experiments that protein delivery and removal by diffusion was

https://doi.org/10.1038/s41467-024-53500-1

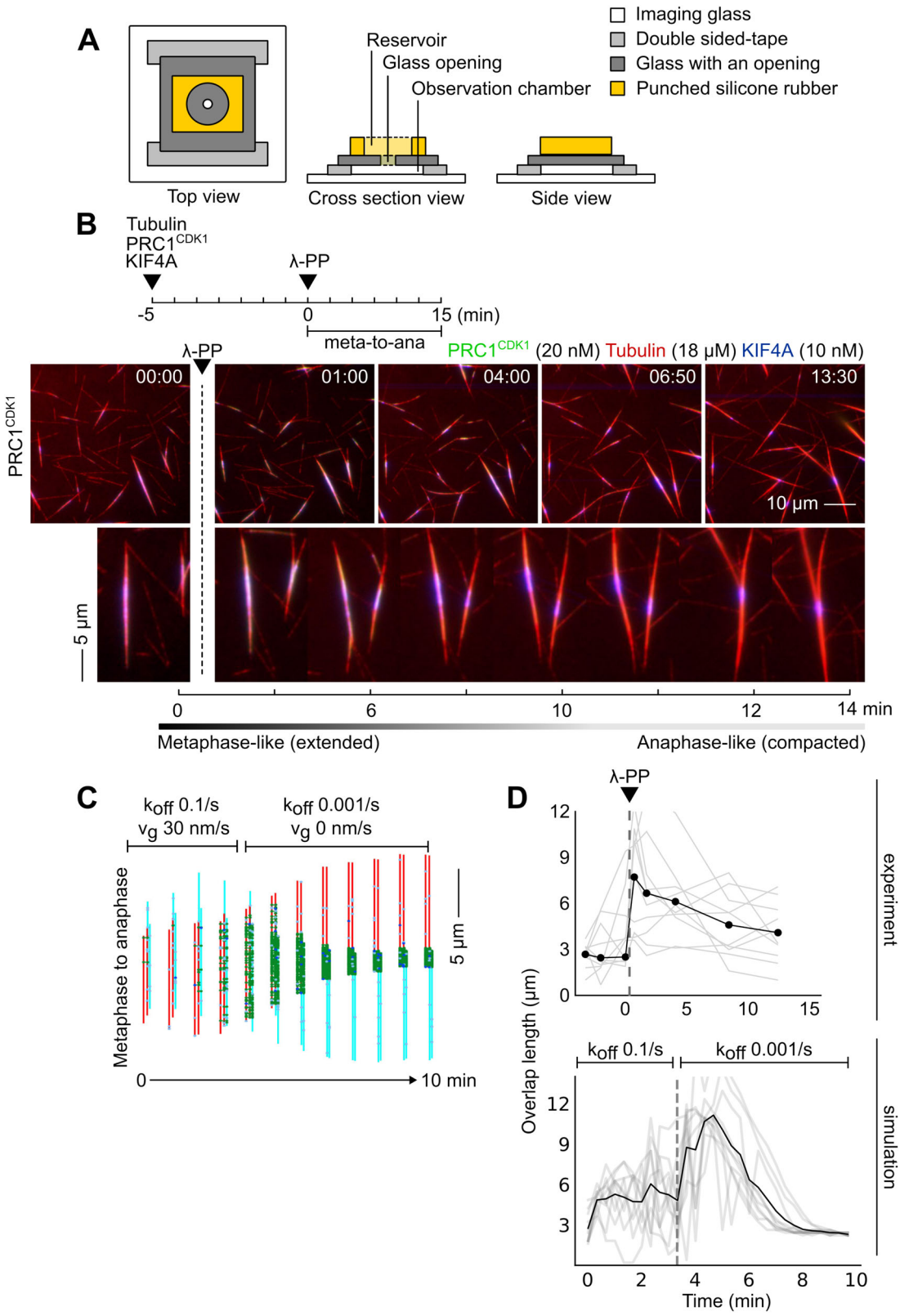

fast enough (within minutes) (Suppl. Fig. 7A). Protein concentrations could be substantially increased and decreased repeatedly without inducing turbulence in the observation chamber (Suppl. Fig. 7B).

Using our new setup allowing protein addition after self-organization (Fig. 4B), we tested if metaphase-like bundles pre-organized in the presence of CDK1-phosphorylated PRC1 and KIF4A can reorganize into anaphase-like bundles with compacted midzones when PRC1 becomes dephosphorylated, mimicking the situation in cells when cyclin B is degraded and PRC1 becomes dephosphorylated as a consequence of decreasing CDK1 and increasing phosphatase activity. To mimic the action of protein phosphatase 2 (PP2)/B55, which dephosphorylates PRC1 during anaphase in cells[44], we used lambda protein phosphatase (λ-PP), which we showed was able to completely dephosphorylate CDK1-phosphorylated PRC1 in vitro

Fig. 4 | Transition of metaphase to anaphase-like microtubule bundle organization. A Schematic top, cross section and side view of a flow chamber with a top reservoir. **B** TIRF microscopy images showing microtubule bundles with antiparallel overlaps that were pre-organized for ~5 min in the presence of 20 nM CDK1-phosphorylated PRC1-Alexa546 (green), 10 nM KIF4A-mGFP (blue) and 18 μM Alexa647-tubulin (red), followed by addition of 500 pM lambda-protein phosphatase (λ-PP), 1 mM $MnCl_2$ and 500 μM RO-3306 to the top reservoir to deliver the phosphatase to the imaging chamber to dephosphorylate PRC1. Times in min:sec, scale bars as indicated. **C** Exemplary snap shot depicts the temporal progression of a simulated antiparallel bundle of 4 microtubules connected by PRC1 (green) and KIF4A (blue), undergoing a transition from metaphase-to-anaphase-like organization. Microtubule orientation is indicated by color (plus ends up: cyan, plus ends down: red). The unbinding rate of PRC1 (k_{off}) and the microtubule plus end growth speed (v_g) were changed as indicated to trigger reorganization. **D** Quantification of average antiparallel overlap length of 10 experimental (top) and 10 simulated (bottom) microtubule bundles as a function of time. The gray dotted lines indicate the time of addition of λ-PP in the experiment, or change of unbinding rate (k_{off}) and microtubule growth speed in the simulation, as indicated. $n = 2$ independent experiments, total of 10 antiparallel overlaps (top), and $n = 10$ independent simulations, total of 10 antiparallel overlaps (bottom). Black and gray lines are mean and individual overlap length, respectively. Source data are provided as a Source Data file.

(Suppl. Fig. 8A). First, mixed polarity microtubule bundles were allowed to organize after combining CDK1-phosphorylated PRC1, KIF4A and tubulin. After ~5 min, when bundles were not excessively long yet (at the conditions of uninhibited plus end growth here), λ-phosphatase was added. Addition of phosphatase to these mixed-polarity bundles with broadly distributed CDK1-phosphorylated PRC1 and KIF4A resulted within minutes in increased binding of PRC1 and KIF4A and a strong compaction of the antiparallel microtubule overlaps as indicated by a more compacted PRC1 and KIF4A localization (Fig. 4B, Supplementary Movie 5). Quantification of the overlap length revealed that after λ-phosphatase addition, the antiparallel overlaps initially increased in length before they compacted to a final length of ~4.1 ± 1.9 um (Fig. 4D, top). These results demonstrate that dephosphorylating CDK1-phosphorylated PRC1 is sufficient to induce a metaphase-to-anaphase-like reorganization of minimal midzones organized by PRC1 and KIF4A.

To investigate this reorganization based on a simple mathematical model, we turned again to computer simulations. The metaphase to anaphase transition was triggered by increasing the affinity of PRC1 after 200 s to mimic the effect of dephosphorylation of PRC1 by the added phosphatase and by stopping at the same time microtubule plus end growth to mimic the effect of additionally recruited KIF4A on microtubule dynamics. As in the experiments, long overlaps, increasingly decorated with PRC1 and KIF4A, formed initially after the parameter change followed by overlap compaction (Fig. 4C, D, bottom). Thus, both the experiment and simulation data demonstrate that increased microtubule binding affinity of PRC1 following dephosphorylation of its CDK1 sites is sufficient to trigger a metaphase-to-anaphase-like re-organization of antiparallel overlaps in the presence of KIF4A, mimicking some aspects of central spindle reorganization at the metaphase-to-anaphase transition in cells.

Minimal midzone reorganizations are reversible

Next, we asked whether also the opposite transition from anaphase to metaphase-like bundles can be triggered in vitro. Approximately 10 - 15 min after the start of minimal midzone self-organization in the presence of unphosphorylated PRC1 and KIF4A, we delivered CDK1/cyclin B/CKS1 by diffusion to the pre-organized antiparallel anaphase-like microtubule bundles with compacted antiparallel overlaps. Shortly after CDK1 delivery, PRC1 partially unbound from the compacted overlaps, consistent with decreasing microtubule binding affinity upon phosphorylation by CDK1. PRC1 unbinding also released KIF4A, leading to an almost complete loss of the compacted overlaps (Fig. 5A, Supplementary Movie 6). At the same time, microtubule bundles elongated (Fig. 5C, top), indicating that microtubules resumed plus-end growth after a major fraction of the growth-inhibiting KIF4A was released from the bundles. These observations emphasize that minimal midzones that are organized by unphosphorylated PRC1 and KIF4A are true steady-state structures that transform into a new structure when conditions change, in our case here when the affinity of PRC1 changes caused by phosphorylation by CDK1. This 'backward' anaphase-to-metaphase reorganization has also been observed in cells, demonstrating that an anaphase cytoskeleton can indeed be reorganized to a metaphase architecture when CDK1 activity is artificially increased in anaphase[6].

The experimentally observed 'backward' anaphase-to-metaphase reorganization could also be reproduced in computer simulations by decreasing the affinity of PRC1 for microtubule binding and by allowing at the same time plus ends to grow again after anaphase-like midzones had formed, resulting in the disappearance of the compact microtubule overlaps. This demonstrates that these two parameters which are expected to change as a consequence of PRC1 phosphorylation and concomitant reduced KIF4A recruitment to microtubule bundles in the experiment are sufficient to induce a backwards anaphase-to-metaphase reorganization (Fig. 5B, C, bottom).

Strong microtubule binding of PRC1 to antiparallel microtubules resists KIF4A-driven sliding in stable minimal midzones

Finally, we triggered two sequential reorganizations of anaphase midzone bundles by first adding CDK1 and later lambda phosphatase. To be able to directly observe the motility of microtubules in antiparallel microtubule bundles during minimal midzone bundle reorganizations, we performed also in addition a tubulin speckle microscopy experiments, under the same conditions, but with microtubules being additionally sparsely labeled with tetramethylrhodamine (TAMRA) and PRC1-Alexa546 being replaced by non-fluorescent PRC1. We then observed the change of organizational state in response to kinase and phosphatase addition. First, we triggered an anaphase-to-metaphase-like transition by adding CDK1 (Fig. 6A). As observed before, PRC1 started to unbind and release KIF4A, resulting in the loss of compacted overlaps and in elongation of the microtubule bundles (Fig. 6A, top two rows). Moreover, TAMRA speckle-labeled microtubules could be observed to start sliding in opposite directions at ~15 ± 10 nm/s (Fig. 6A, bottom). Next, we triggered a transition to an anaphase-like state by dephosphorylating PRC1 by adding λ-phosphatase. This could to a certain extent compact midzones again. PRC1 increasingly bound to the microtubule bundles again, recruiting also more KIF4A (Fig. 6A, top two rows). The two proteins initially bound all along the bundles and then started to concentrate again locally. TAMRA speckle-labeled microtubules slid now only very slowly at ~1 nm/s as dephosphorylated PRC1 became concentrated at the newly formed compacted midzones (Fig. 6A, bottom row). Collectively, these results demonstrate that the ability of KIF4A to slide PRC1 bundled microtubules decreases as the degree of PRC1 phosphorylation by CDK1 decreases during the metaphase to anaphase transition.

This stronger resistance to KIF4A-driven microtubule sliding by non-phosphorylated PRC1 compared to CDK1-phosphorylated PRC1 could also be demonstrated by first allowing antiparallel microtubule bundles to self-organize for ~10 min in the presence of either CDK1-phosphorylated or unphosphorylated PRC1-Alexa546 followed by introducing KIF4A-mGFP. First, antiparallel microtubule overlaps were allowed to form in the presence of CDK1-phosphorylated PRC1, now with growing microtubule plus end out due to faster plus end

https://doi.org/10.1038/s41467-024-53500-1

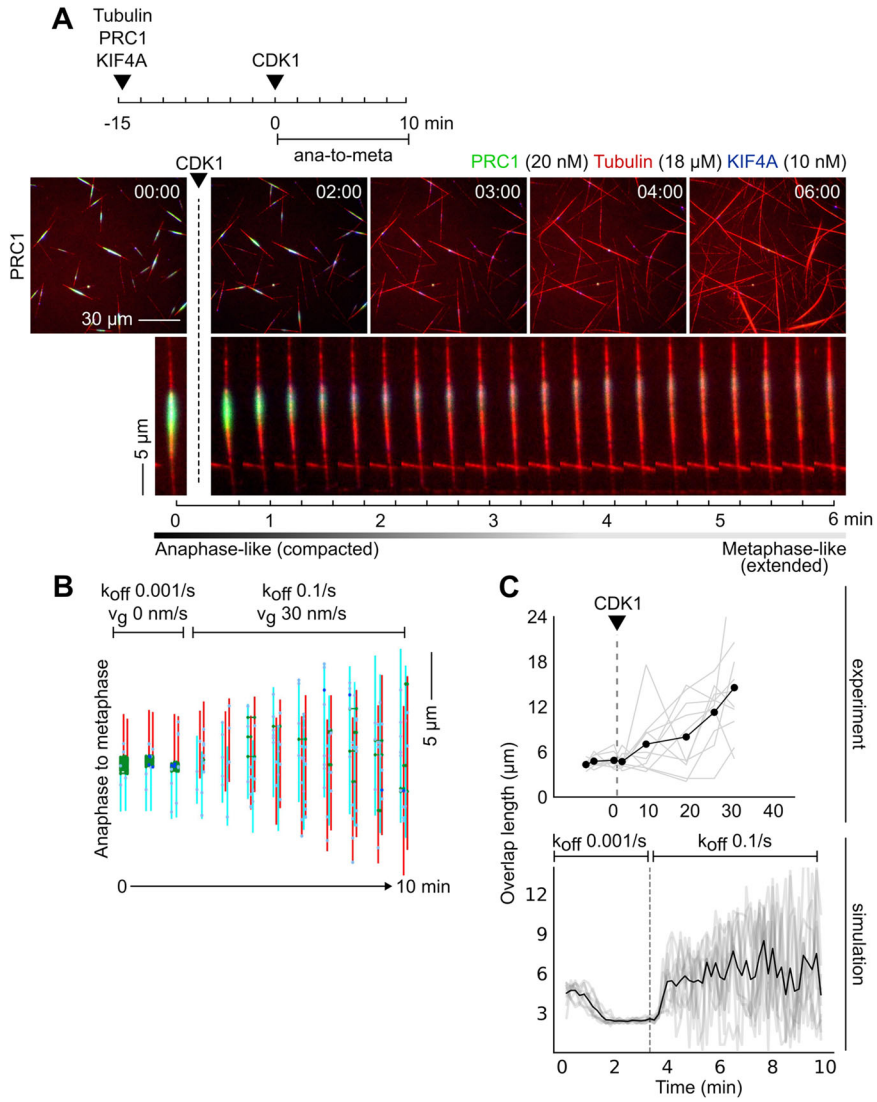

Fig. 5 | Backward transition from anaphase to metaphase-like microtubule bundle organization. A TIRF microscopy images showing microtubule bundles pre-organized for ~10–15 min in the presence of 20 nM unphosphorylated PRC1-Alexa546 (green), 10 nM KIF4A-mGFP (blue) and 18 μM Alexa647-tubulin (red), followed by addition of 100 nM CDK1/cyclin B/CKS1 to the top reservoir for delivery to the imaging chamber to phosphorylate PRC1. A large fraction of PRC1 and KIF4A was lost within minutes from the compacted antiparallel overlaps. Times in min:sec, scale bars as indicated. **B** Exemplary snap shot depict the temporal progression of simulated antiparallel bundles of 4 microtubules connected by PRC1 (green) and KIF4A (blue), undergoing a transition from anaphase-to-metaphase-like organization. Microtubule orientation indicated by color (plus ends up: cyan, plus ends down: red). The unbinding rate of PRC1 (k_{off}) and the microtubule plus end growth speed (v_g) were changed as indicated to trigger reorganization. **C** Average antiparallel overlap length of 10 experimental (top) and 10 simulated (bottom) microtubule bundles as a function of time. The gray dotted lines indicate the time of addition of CDK1/cyclin B/CKS1 in the experiment, or change of unbinding rate (k_{off}) and microtubule growth speed in the simulation, as indicated. $n = 2$ independent experiments, total of 10 antiparallel overlaps (top), and $n = 10$ independent simulations, total of 10 antiparallel overlaps (bottom). Black and gray lines are mean and individual overlap length, respectively. Source data are provided as a Source Data file.

growth in the absence of KIF4A (Fig. 6B left). After KIF4A addition, KIF4A-driven antiparallel microtubule sliding started at ~30 ± 10 nm/s, as shown in the tubulin speckle experiment (Fig. 6B, bottom), mixing up the microtubules in the bundles, thereby 'dissolving' the local accumulation of PRC1 and KIF4A (Fig. 6B, two top rows, Supplementary Movie 7). Conversely, bundles that were formed in the presence of unphosphorylated PRC1 (also with growing plus ends out) resisted sliding, moving at only ~0.2 nm/s, when KIF4A was added (Fig. 6C, Supplementary Movie 7). These results provide further evidence that unphosphorylated PRC1 indeed supports minimal midzone organization and stability by providing more resistance against KIF4A-driven microtubule sliding, likely due to a higher PRC1 density in the overlaps.

In conclusion, controlling the CDK1-phosphorylation state of PRC1 is sufficient to control the organizational state of PRC1 and KIF4A containing self-organized minimal midzone bundles.

Discussion

We report here the in vitro reconstitution of kinase/phosphatase-controlled reorganizations of self-organized microtubule networks. We investigated a minimal system consisting of dynamic microtubules and two prominent human midzone proteins. Although the phase space of self-organization of these proteins is rich[38,45,46], here we focused on microtubule assemblies that mimic metaphase or anaphase-like central spindle architectures. Regulatory control is exerted by changing the phosphorylation state of a key network

https://doi.org/10.1038/s41467-024-53500-1

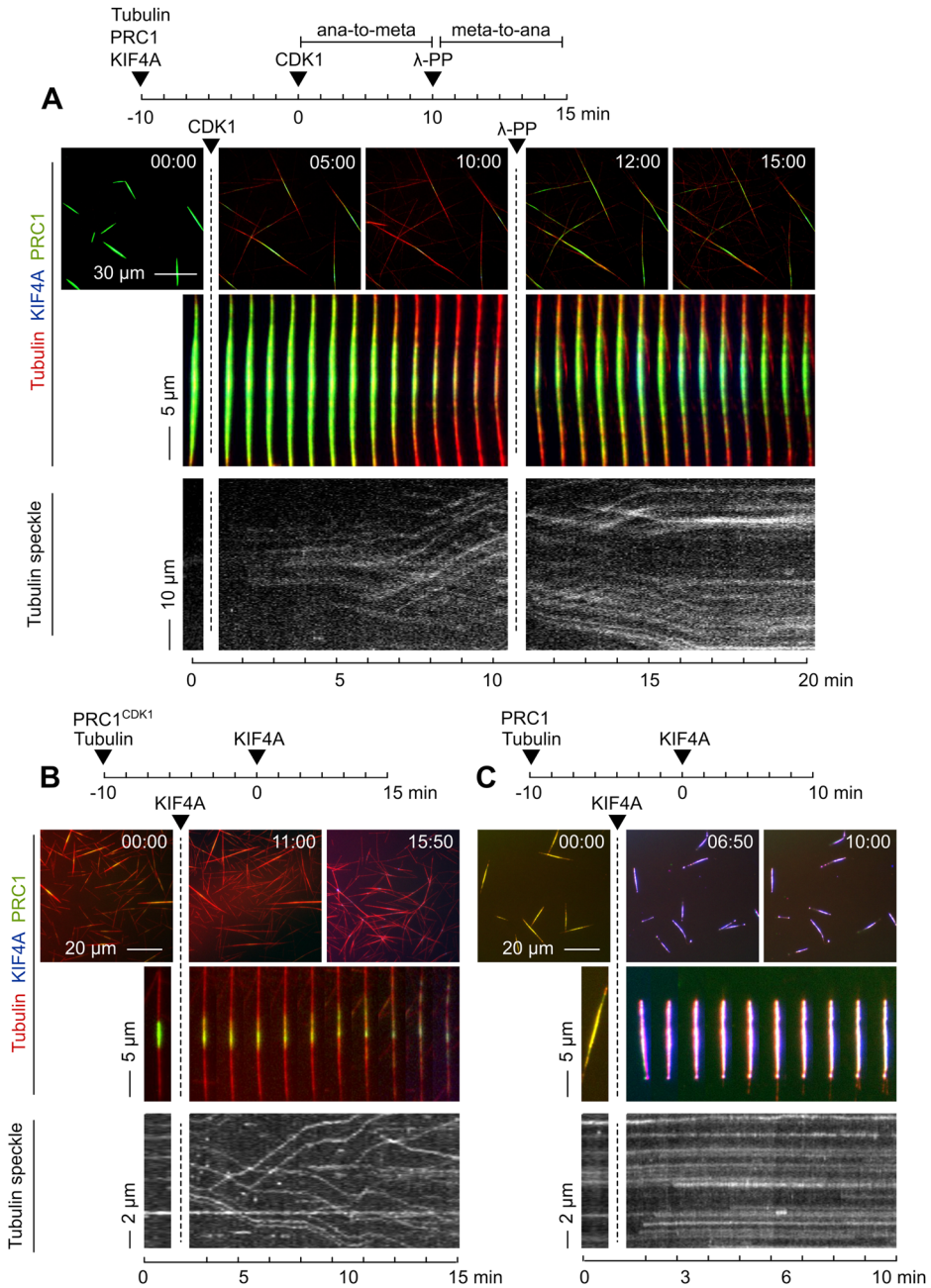

Fig. 6 | KIF4A-driven sliding is more evident in minimal midzones organized by CDK1-phosphorylated PRC1. A TIRF microscopy images of microtubule bundles transitioning from an anaphase-to-metaphase-like organization (as in Fig. 4), followed by metaphase-to-anaphase-like transition (as in Fig. 5) using 18 μM Alexa647-tubulin (red), 20 nM PRC1-Alexa546 (green) and 10 nM KIF4A-mGFP (blue). Upon addition of 100 nM CDK1/cyclin B/CKS1, a large fraction of PRC1 and KIF4A detached rapidly from the compacted antiparallel overlaps and the bundles extended, mimicking an anaphase-to-metaphase-like transition. After 10 min, 500 pM λ-PP, 1 mM $MnCl_2$ and 500 μM CDK1 inhibitor RO-3306 were added to the reservoir to dephosphorylate PRC1 which caused PRC1 and KIF4A to rebind and antiparallel overlaps first extend before they contracted, mimicking a metaphase-to-anaphase transition. Kymograph of TAMRA-tubulin speckles from a microtubule bundle organized at the same condition as in the images above, but using unlabeled PRC1 and additional 0.9 μM of TAMRA-tubulin (bottom). TAMRA-tubulin speckle velocity after CDK1 addition was ~ 1 nm/s initially and later 15 ± 10 nm/s after PRC1 was phosphorylated. $n = 2$ independent experiments, 36 and 31 speckles, respectively. In contrast, after λ-PP addition the speckle velocity was first 20 ± 9 nm/s, then ~1 nm/s after PRC1 was dephosphorylated. $n = 2$ independent experiments, 25 and 17 speckles, respectively. **B**, **C** TIRF microscopy images showing microtubule bundles with antiparallel overlaps that were pre-organized for 10 min in the presence of (**B**) 20 nM CDK1-phosphorylated PRC1 or (**C**) 20 nM of unphosphorylated PRC1 (green) and 18 μM Alexa647-tubulin (red), followed by addition of 30 nM KIF4A-mGFP (blue) to the top reservoir and for delivery to the microscopy chamber by diffusion (top). Kymographs of TAMRA-tubulin speckles generated from TIRF microscopy images of microtubule bundles organized at the same conditions as in images above, but using unlabeled CDK1-phosphorylated PRC1 and additional 0.9 μM TAMRA-tubulin (bottom). TAMRA-tubulin speckle velocity in (**B**) is 30 ± 10 nm/s and (**C**) is 0.2 nm/s. $n = 2$ independent experiments, 42 and 26 speckles, respectively. Times in min:sec, scale bar as indicated. Source data are provided as a Source Data file.

component, mimicking a cell cycle-driven transition of the spindle architecture in mitosis.

Our results provide insight into the molecular mechanisms translating kinase or phosphatase action into spatio-temporal network reorganizations of the spindle. We found that the two mitotic kinases CDK1 and PLK1 differentially affect PRC1's biochemical activity. CDK1 controls the affinity of PRC1 for antiparallel microtubule binding, in agreement with a previous microtubule co-sedimentation experiment[9] and explaining why PRC1 accumulates at the central spindle in anaphase when its CDK1-phosphorylation sites become dephosphorylated[11,27,28]. In contrast, PLK1 does not affect the microtubule binding affinity, but instead controls its own recruitment by PRC1, in agreement with observations in cells[27], so that PLK1 can locally regulate events required for cytokinesis[47]. The positions of the phosphorylation sites of both kinases appear to be optimized for their distinct biochemical functions in the context of midzone organization. Our results thus provide a biochemical framework for how phosphorylation of PRC1 by these two kinases are translated into different microtubule network architectures in cells.

We found that the two kinases do not affect each other's ability to phosphorylate PRC1 in solution. In cells, however, phosphorylation of PRC1 by CDK1 was reported to be inhibitory for phosphorylation by PLK1[27]. This could be an indirect effect[30], given that we found that locally concentrating PRC1 and PLK1 in microtubule bundles increases the efficiency of PRC1 phosphorylation by PLK1. A reduced local accumulation of PRC1 and PLK1 in the spindle midzone due to weaker microtubule binding and bundling by CDK1-phosphorylated PRC1 in metaphase could indirectly reduce the efficiency of PRC1 phosphorylation by PLK1. In anaphase, local accumulation of PRC1 after CDK1 sites have been dephosphorylated and of PLK1 bound to PLK1-phosphorylated PRC1 would then lead to further phosphorylation of PRC1 by PLK1 as it accumulates in the midzone.

In our minimal in vitro reconstitution with PRC1 and KIF4A, changing the CDK1-phosphorylation state of PRC1 was sufficient to drive reorganizations between bundles with extended metaphase-like overlaps and compacted anaphase-like overlaps, recapitulating a previous experiment in cells where spindles transitioned back and forth between metaphase and anaphase by manipulating CDK1 activity[6]. Computer simulations demonstrated that changes in PRC1 affinity and in the microtubule growth-inhibiting effect of PRC1-recruited KIF4A are sufficient to explain the reversibility of minimal midzone reorganization. Because active microtubule network reorganizations are in principle reversible, our results also emphasize the importance of the cell cycle controlling the unidirectionality of these reorganizations. It does so by controlling the affinity of a protein with a key microtubule organizing activity that at the same time serves as a hub for protein-protein interactions[3].

Decreasing the microtubule binding affinity of PRC1 by CDK1-mediated phosphorylation does not only decrease PRC1's density in antiparallel microtubule overlaps. It also allows antiparallel microtubules to be transported more easily within bundles by motors, as we showed here for KIF4A. This agrees with previous in vitro experiments that showed that removing the unstructured C-terminal part of PRC1, thereby weakening its affinity for microtubules, allowed more efficient microtubule sliding in mixed polarity bundles of nematic networks by artificial kinesin-1 oligomers[48].

In cells, a low resistance to motor driven microtubule sliding by CDK1-phosphorylated PRC1 in metaphase is a useful property given that in many metaphase spindles microtubules slide outward towards the poles (microtubule flux) driven by the plus end directed motors KIF11 and KIF4A[1]. In anaphase, the CDK1 sites of PRC1 become then gradually dephosphorylated[7,27,28,44], likely initially allowing the spindle architecture to become reorganized, at least in part, still by motor-driven microtubule sliding. At later stages when PRC1 increasingly accumulates in the central spindle due to its increased affinity, it will increasingly resist motor-driven sliding[38,49], leading to the well-characterized compaction of the central spindle observed in cells[15,19].

KIF4A recruitment to the central spindle in early anaphase in cells also requires its release from chromosomes, an interaction that is controlled by Aurora kinases[50] and CDK1[51]. Because the regions in KIF4A for binding to condensin on chromosomes and to PRC1 are in close proximity and may partially overlap[20,49], it is possible that these kinases also regulate the interaction between KIF4A and PRC1, adding a potential additional layer of regulation to midzone organization that will be interesting to investigate in the future.

Our work demonstrates the feasibility of in vitro reconstituting cell-cycle dependent transitions between self-organized microtubule networks. This development paves the way to the study of the molecular requirements of reorganizations of more complex subsystems of the mitotic spindle, containing additional components such as spindle poles and kinetochores and a more complex interplay between kinases and phosphatases, mimicking cell cycle progression ever more faithfully.

Methods

Molecular cloning

To generate an expression construct of SNAP-tagged human PRC1 isoform 2 (NM_199413)[27] (His-TEV-PRC1iso2-SNAP), site directed mutagenesis of a PRC1 isoform 1 (NM_003981.2) containing baculovirus construct (pFF01)[38] was performed to delete the amino sequence KDPSLSDSSTVGLQ that distinguishes the two isoforms. mGFP-tagged human KIF4A (NM_012310.2)[38] (His-TEV-KIF4A-mGFP), and CDK1/cyclin B1/CKS1 (GST-3C-CDK1, His-TEV-Cyclin-B, His-TEV-CKS1)[41] were expressed from existing constructs. To generate a bacterial expression construct for human PLK1 (Uniprot: P53350) that is phosphorylated by Aurora A during expression, a sequence encoding 6xHis-MBP-(TEV)-hPLK1 (MBP-PLK1) was subcloned in a pETDuet-1 vector together with a chimera of human Bora (Uniprot: Q6PGQ7-1, residues 18-120) and full length human Aurora A-GFP, where Aurora A (Uniprot: O14965) and GFP are separated by six "GGGS" repeats. To generate a baculovirus expression construct for PLK1 that is phosphorylated by Aurora A during expression in insect cells, cDNAs encoding 6xHis-(TEV)-hPLK1 and the Aurora-Bora chimera described above were subcloned in pLIB vectors[52]. The construct for bacterial expression of GFP contained sequences encoding a Z-tag, a TEV cleavage site, a preScission cleavage site, mGFP, and an oligohistidine tag in the stated order in pETMZ.

Protein expression and purification

The human PRC1 isoform 2 construct was expressed in Sf21 cells (Thermo Fisher Scientific) and was purified from a 500 mL culture grown in suspension at 27 °C in Sf-900 III SFM (1x) Serum Free Medium (Gibco). The PRC1 purification was carried out on ice or at 4 °C. Harvested cells were resuspended by douncing in Lysis Buffer (50 mM NaPi, 500 mM KCl, 2 mM imidazole, 3 mM EDTA, 10 mM 2-mercaptoethanol (ME), 0.2 mM ATP, pH 7.5) supplemented with protease inhibitor (Roche). The lysate was clarified by ultracentrifugation (183,632 g, 30 min), incubated with 1.5 g of Ni-TED resin (Macherey-Nagel) for 2 h, then loaded into a gravity column. PRC1 was eluted using Elution Buffer (50 mM NaPi, 500 mM KCl, 400 mM imidazole, 3 mM EDTA, 10 mM ME, pH 7.5), subsequently buffer exchanged into Gel Filtration Buffer (50 mM NaPi, 500 mM KCl, 3 mM EDTA, 2 mM DTT, pH 7.5), followed by proteolytic removal of the oligohistidine tag and a final size exclusion chromatography step[38], yielding ~ 1 mg of PRC1-SNAP in Gel Filtration Buffer. To generate fluorescently labeled PRC1-Alexa546, the SNAP tag was labeled with SNAP-Surface Alexa Fluor-546 (NEB) during cleavage of the oligohistidine tag.

KIF4A-mGFP was expressed in Sf21 cells from an existing baculovirus construct and was purified from a 500 mL culture as described for PRC1 but using the following buffers: Lysis Buffer (50 mM NaPi, 350 mM KCl, 2 mM imidazole, 1 mM $MgCl_2$, 1 mM EDTA, 10 mM ME,

0.2 mM ATP, 50 mM glutamate, 50 mM arginine, pH 7.5); Elution Buffer (50 mM NaPi, 350 mM KCl, 300 mM Imidazole, 1 mM $MgCl_2$, 1 mM EDTA, 10 mM ME, 0.2 mM ATP, 50 mM glutamate, 50 mM arginine, pH 7.5); Gel Filtration Buffer (50 mM NaPi, 350 mM KCl, 1 mM $MgCl_2$, 1 mM EDTA, 2 mM DTT, 0.2 mM ATP, 50 mM glutamate, 50 mM arginine, pH 7.5)[38], yielding typically 1 mg of KIF4A-mGFP in Gel Filtration Buffer.

CDK1/cyclin B1/CKS1 was co-expressed in insect cells with CDK-activating kinase (CAK) from S. cerevisiae (CIV1) to activate CDK1 by phosphorylation on the activation loop and was purified as described[41].

To express MBP-PLK1, *Escherichia coli* Rosetta DE3 were transformed via heat shock. Transformed cells were incubated overnight in a liquid pre-culture containing ampicillin (100 µg/mL). The next day, a small volume of the transformed cells (1/1000 of the culture volume) was used to inoculate 2 L of terrific broth (TB) medium supplemented with ampicillin (100 µg/mL). Cells were grown to an optical density (OD) = 0.8 before induction of protein expression with 0.1 mM IPTG. Expression of the protein continued for 16 h at 18 °C. Cells were pelleted and snap-frozen, to be stored at −80 °C until purification. Cells were resuspended in purification buffer (50 mM HEPES 7.5, 300 mM NaCl, 5 % glycerol, 1 mM TCEP) further supplemented with DNAse I (Roche) and Protease Inhibitor Cocktail (Serva). After sonication for cell lysis, the total lysate was subjected to centrifugation at 80,000 *g* for 45 min. The supernatant was syringe-filtered (0.45 µM cutoff) and applied onto a 5-mL MBP trap column (Cytiva) for 2 h at a constant flow of 2 mL/min. Bound proteins were washed by applying 14 column volumes (CV) of purification buffer. Elution was performed in a single step using 10 mM maltose resuspended in purification buffer. The eluted protein was then applied at constant flow onto a 5-mL GSH column (Cytiva), pre-equilibrated and previously loaded with a GST-GFP nanobody (8 mg, produced in house) to capture Bora-Aurora-GFP leftovers. After an 18-h incubation, the flow-through containing MBP-PLK1 was collected, concentrated with an Amicon concentrator (50 kDa cutoff) and injected onto a Superdex 200 16/600 size exclusion chromatography column pre-equilibrated in purification buffer. The purest fractions corresponding to the soluble part of the protein were collected, pooled and concentrated up to a suitable concentration (typically 30–40 µM), then aliquoted, snap-frozen and stored at −80 °C.

For expression of His-PLK1, *Sf9* cells (Thermo Fisher Scientific) were infected for 3-4 days and added (1:20 dilution) to logarithmically growing *Hi5*-derived *Tnao38* insect cells in 1 L Sf9-II medium (ThermoFisher Scientific)[53]. All insect cell cultures were grown at 27 °C. Cells were harvested after 3 days by centrifugation at 1000 *g* at room temperature, washed once with ice-cold PBS, pelleted by centrifugation at 1000 *g* at 4 °C, flash-frozen in liquid nitrogen, and stored at −80 °C. Resuspension of cells in purification buffer was followed by sonication and centrifugation at 80,000 *g* for 45 min. Cleared lysate was pump-filtered (0.45 µM cutoff) and applied onto a 5 mL HisTrap Talon column at constant flow for 2 h. After a brief wash, the bound protein was incubated with cleared lysate expressing the Bora-Aurora chimera, supplemented with 3 mM ATP and 10 mM $MgCl_2$ for 16 h. After extensive washes, bound proteins were eluted by gradient elution up to 300 mM imidazole, and the purest fractions were isolated. The sample was diluted with buffer A (50 mM HEPES 7.5, 5 % glycerol, 1 mM TCEP) up to 25 mM NaCl final concentration and then loaded on a Resource Q anion exchange chromatography column (Cytiva) pre-equilibrated in buffer A. The sample was eluted with a linear gradient of 25-500 mM NaCl in 11 bed column volumes. Fractions containing His-PLK1 and devoid of Aurora-Bora leftover were pooled, concentrated and loaded onto a Superdex 200 16/60 SEC column (Cytiva) pre-equilibrated in purification buffer. Fractions containing His-PLK1 were concentrated, flash-frozen in liquid nitrogen and stored at 80 °C. All purification steps were performed on ice or at 4 °C.

To express lambda protein phosphatase (Uniprot: P03772), a pET28 vector scaffold expressing recombinant phosphatase was used to transform *Escherichia coli* strain C41 (DE3) via heat shock. Protein expression was performed in 1 L TB medium supplemented with kanamycin (50 µg/mL), and was induced by addition of 0.5 mM IPTG at OD = 0.6–0.8. Cells were incubated for 16 h at 18 °C, harvested by centrifugation, and pellets frozen at −80 °C for storage. Cell lysis was performed via high-pressure homogenization (Cell Disruptor) at 1.35 kbar after resuspension in lysis buffer (25 mM HEPES pH 7.5, 300 mM NaCl, 5 mM imidazole, 1 mM TCEP, 10% glycerol, DNAse mix and Roche EDTA-free protease inhibitor cocktail). For protein purification, the lysate was centrifuged at 80,000 *g* for 30 min at 4 °C. The resulting supernatant was loaded on a 5 mL HisTrap Talon column (Cytiva). The column was washed extensively and bound proteins were eluted in 25 mM HEPES pH 7.5, 300 mM NaCl, 1 mM TCEP, 10% glycerol, 200 mM imidazole. Lambda protein phosphatase was concentrated and injected on a HiLoad 26/60 Superdex 75 column (Cytiva). The purest fractions were collected, concentrated, aliquoted and snap-frozen. The protein was stored at -80 °C prior to the experiments.

Porcine brain tubulin was purified as described[54]. Labeling of purified tubulin with Alexa647-N-hydroxysuccinimide ester (NHS; Sigma-Aldrich), or biotin-NHS (Thermo Scientific) was performed as described[55]; the labeling ratio was kept below 0.2 dye per tubulin heterodimer to preserve the tubulin activity as best as possible. All tubulin variants were stored in BRB80 (80 mM PIPES, 1 mM EGTA, 1 mM $MgCl_2$, pH 6.8).

GFP was expressed for 3 h at 37 °C in BL21-CodonPlus(DE3)-RIL grown in Luria Bertani (LB) media supplemented with kanamycin and chloramphenicol and was purified from a 2 L culture using metal affinity chromatography (HisTrap FF, 5 mL, Cytiva, equilibrated with GFP binding buffer (50 mM Tris-HCL, 400 mM KCl, 2 mM $MgCl_2$, 10 mM imidazole, 1 mM ME, 0.001 % Brij-35)), followed by proteolytic removal of the oligohistidine tag and a final step of size exclusion chromatography (HiLoad Superdex 200 16/600, equilibrated in storage buffer (50 mM Tris-HCl, 200 mM KCl, pH 8)). The resulting yield is ~ 8 mg GFP in storage buffer.

All protein concentrations were determined by measuring the absorbance at 280 nm using a NanoDrop ND-1000 spectrophotometer. A Coomassie stained SDS-PAGE gel with the purified proteins used in this study is shown in Suppl. Fig. 8B.

Fluorescence labeling of PLK1

To remove the N-terminal tag while generating an N-terminal glycine for sortase labeling, His-PLK1 (25 µM) was incubated in a reaction volume of 50 µL with sub-stoichiometric concentrations (1:20 ratio with PLK1) of His-MBP-TEV protease. Purified Sortase A 7 + [56] (produced in house) was added at 10 µM together with a 6-Carboxyfluorescein (FAM)-labeled LPETGG peptide (Genscript) at 500 µM. After a 16-h incubation at 4 °C, the sample was injected onto a Superdex 200 5/150 column (Cytiva) connected to an Äkta Micro FPLC system (Cytiva) to remove the excess of peptide and separate Sortase and His-MBP-TEV protease from fluorescein-PLK1.

Phosphorylation of purified PRC1 by purified kinases

Unlabeled PRC1-SNAP was phosphorylated by CDK1/cyclin B/CKS1 or by MBP-PLK1 (for all experiments except analytical size exclusion chromatography (SEC)) or by His-PLK1 (for analytical SEC, Fig. 1D, E) at 4 °C in kinase buffer (50 mM NaPi, 10 mM $MgCl_2$, 150 mM KCl, 2 mM ATP, 5 mM ME, pH 7.5). Protein concentrations were 5 µM PRC1, 170 nM ternary CDK1 complex or 1 µM PLK1. Phosphorylations were performed at a cold temperature and high kinase concentrations in order to minimize the duration of phosphorylation needed for complete phosphorylation to best preserve PRC1 activity before using it in microscopy-based self-organization experiments.

For time course measurements, the incubation times varied between 5 to 40 min until the reaction was stopped by adding SDS-containing sample buffer. The samples were analyzed either using Phos-tag SDS-PAGE, Pro Diamond Q staining of SDS gels, or by quantitative mass spectroscopy of gel-excised protein bands.

For TIRF microscopy experiments, 5 μM PRC1-Alexa546 was phosphorylated by either 170 nM CDK1/Cyclin B/CKS1 or 1 μM PLK1-MBP at 4 °C in kinase buffer for 5 min or 30 min, respectively, before the reaction was stopped by adding 500 μM either kinase inhibitor RO-3306 or BI-2536, respectively.

Dephosphorylation of CDK1-phosphorylated PRC1

To measure the time course of PRC1 dephosphorylation, 0.8 μM CDK1-phosphorylated PRC1, generated by incubating 5 μM PRC1-SNAP with 170 nM CDK1/cyclin B/CKS1 at 4 °C in kinase buffer for 5 min and then adding 500 μM RO-3306, was dephosphorylated by 1.2 μM to 10 μM lambda protein phosphatase (Lambda PP) at 30 °C for 5 to 60 min, either in PRC1 storage buffer or microscopy buffer AB (see below), as indicated in the figures and figure legends. The reaction was stopped by the addition of SDS-containing sample buffer and the samples were analyzed using Phos-tag SDS-PAGE and Pro-Q Diamond phosphoprotein staining of standard SDS gels.

Analysis of degree of phosphorylation of PRC1 by SDS-PAGE

5 μg or 800 ng phosphorylated PRC1 per lane was separated on a hand-casted 7.5% SDS-polyacrylamide gel supplemented with Phos-tag reagent (NARD Institute). The gel was stained with either Coomassie Blue or SYPRO Ruby and imaged using an iBright FL1500 Imaging System (Invitrogen) or Gel Doc XR+ System (BioRad).

Alternatively, 5 μg phosphorylated PRC1 per lane was separated on a 4-20% gradient SDS-polyacrylamide gel (BioRad) and stained with Pro-Q Diamond phosphoprotein stain (Invitrogen). The gel was imaged using an iBright FL1500 (Invitrogen). The same gel was subsequently stained with Coomassie Blue stain.

Quantitative mass-spectrometry

Sample preparation. 5 μg phosphorylated PRC1 per lane was separated by a 3-8% gradient SDS-polyacrylamide gel (BioRad) and stained with Coomassie Blue. The protein bands of interest were excised. Gel bands were destained with NH_4HCO_3 (100 mM) in 40% acetonitrile, reduced in dithiothreitol (2 μmol, 20 min, 56 °C), and alkylated with iodoacetamide (11 μmol, 30 min, 25 °C). Next, proteins were digested with either LysC (400 ng, Wako, cat # 129-02541) or trypsin (400 ng, Promega cat # V5113) for overnight at 37 °C. After digestion, the peptide mix was acidified with formic acid and desalted with a MicroSpin C18 column (The Nest Group, Inc).

Chromatographic and mass spectrometric analysis. For quantitative determination of kinase-dependent phosphorylation of PRC1 residues by CDK1 (T470, T481 & S513) and PLK1 (T578 & T602), a known amount of C-terminally isotopic labeled synthetic peptides ($^{13}C_6$,$^{15}N_4$-Arg, $^{13}C_6$,$^{15}N_2$-Lys) was spiked in the samples and used to estimate the absolute amount of the endogenous peptides. Samples were analyzed by LC-MS using an Orbitrap Fusion Lumos (Thermo Fisher Scientific) coupled to an EASY-nLC 1200 (Thermo Fisher Scientific).

Peptides were loaded directly into the analytical column and separated by reverse-phase chromatography (50-cm × 75 μm C18 column, 2 μm) with gradients ranging from 4 to 45% 48% in 60 min.

The mass spectrometer in data-dependent acquisition (DDA) mode. In each cycle of data-dependent acquisition analysis, following each survey scan, the most intense ions above were selected for fragmentation via high-energy collision dissociation (HCD) at normalized collision energy of 28%. QCloud was used to control the instrument longitudinal performance throughout the analysis[57].

Data Analysis. The acquired spectra were analyzed using the Proteome Discoverer software suite (v2.5, Thermo Fisher Scientific) and the Mascot search engine (v2.6, Matrix Science). The data were searched against a Swiss-Prot human database (as in February 2020, 20365 entries) and PRC1 isoform 2 (O43663), a list of common contaminants and all the corresponding decoy entries. For peptide identification a precursor ion mass tolerance of 7 ppm was used for MS1 level, trypsin was chosen as enzyme and up to three missed cleavages were allowed. The fragment ion mass tolerance was set at 0.5 Dalton for MS2 spectra. Phosphorylation of serine, threonine and tyrosine, oxidation of methionine and N-terminal protein acetylation were used as variable modifications whereas carbamidomethylation on cysteines was set as a fixed modification. False discovery rate (FDR) in peptide identification was set to a maximum of 1%. Skyline software 5 (23.0.9.187) was used to generate the library (output of Proteome Discoverer search) and extract the areas of each peptide.

Analytical size-exclusion chromatography

To test whether there is a strong interaction between PRC1 and the CDK1 complex or His-PLK1, we used analytical SEC. A mixture of 5 μM PRC1 and 3 μM CDK1 complex with 2 mM ATP (in kinase buffer, incubated 5 min), or a mixture of 5 μM PLK1 with or without 2 mM ATP (in kinase buffer, incubated 30 min), and for comparison the individual proteins at the same respective concentrations were run through a Superdex 200 increase 5/150 GL or Superose 6 increase 5/150 GL column (Cytiva) equilibrated in PRC1 storage buffer. All samples were eluted under isocratic conditions at 4 °C at a flow rate of 0.18 mL/min. Protein elution was monitored by absorbance measurement at 280 nm. Proteins fractions (100 μL) were collected and analyzed by SDS-PAGE and Coomassie Blue staining.

Dynamic antiparallel microtubule pairs

Flow chambers were assembled from a biotin-PEG functionalised glass (10% biotin-PEG-NH2 and 90% HO-PEG-NH2; Rapp Polymere) and a PLL-PEG passivated counter glass separated by two stripes of double-sided sticky tape[55].

The following solutions were flowed through the chamber at room temperature, each time 10 chamber volumes (~50 μL), if not indicated otherwise:

(1) 1% Pluronic F-127 in deionized water (incubated for 10 min before the next flow).

(2) 30 chamber volumes β-AB (50 μg/mL β-casein in AB (80 mM PIPES, 85 mM KCl, 85 mM KOA, 4 mM $MgCl_2$, 1 mM GTP, 2 mM ATP, 1 mM EGTA, 10 mM ME, 0.005% (w/v) Brij-35, 33 mM glucose, 0.15% (w/v) methylcellulose, pH 6.8)).

(3) 50 μg/mL Neutravidin in β-AB (3 min incubation).

(4) AB (β-AB without β-casein).

(5) GMPCPP-stabilized biotinylated and fluorescently-labeled microtubules seed were prepared as previously described[23].

(6) BRB80 (80 mM PIPES, 1 mM $MgCl_2$, 1 mM EGTA, pH 6.8).

(7) AB.

(8) Final solution: 18 μM tubulin (a composite of unlabeled and Alexa647-tubulin with a final labeling ratio of ~ 0.1) and 5 - 100 nM unphosphorylated or phosphorylated PRC1-Alexa546 diluted into AB, supplemented with oxygen scavengers (320 μg/mL glucose oxidase (Serva), 55 μg/mL catalase (Sigma-Aldrich)), and ultra-centrifuged (278.088 g, 15 min, 4 °C) just before the experiment. In some experiments, the final solution contained additionally 12–100 nM PLK1-FAM to be able to monitor binding of PLK1 to antiparallel microtubule overlaps.

The chamber was sealed with vacuum grease (Beckman Colter) and the immobilized microtubules were imaged at 30 °C on a TIRF microscope (dual color imaging, see below). Alexa647-microtubules grew dynamically from immobilized GMPCPP-microtubules and

occasionally formed antiparallel overlaps to which PRC1 bound preferentially, as reported previously[23]. The PRC1-Alexa546 fluorescence intensity in these overlaps was quantified to generate binding curves (see below).

PRC1/KIF4A end tags

To observe PRC1/KIF4A end tags at the plus ends of individual immobilized microtubules, flow chambers were constructed and the same sequence of solutions were flowed through as described for the 'Dynamic antiparallel microtubule pair assay', however with the following changes:

(i) AB and β-AB were replaced by AB2 and β-AB2 (AB and β-AB prepared without KCl).

(ii) The final solution contained in addition to 10 nM PRC1-Alexa546 also 5–30 nM KIF4A-mGFP, and 10 μM tubulin (a composite of unlabeled and Alexa647-tubulin with a final labeling ratio of ~0.1).

The chamber was sealed as above and imaged at 30 °C on a TIRF microscope (triple color imaging, see below). Microtubules grew dynamically from both ends of the immobilized GMPCPP-microtubules, unless PRC1/KIF4A end tags formed which stopped plus end growth, as reported previously[31].

Self-organization of minimal anaphase midzones

10 chamber volumes, unless stated otherwise, of the following solutions were flowed through a flow chamber (prepared as described above) at room temperature:

(1) 1% Pluronic F-127 (10 min)

(2) 30 chamber volumes of β-AB2

(3) AB2

(4) Final solution containing 5 - 20 nM PRC1-Alexa546, 5 - 100 nM KIF4A-mGFP, 18 μM unlabeled and Alexa647-tubulin (10% final average labeling ratio) diluted into Buffer AB2, supplemented with oxygen scavengers (320 μg/mL glucose oxidase (Serva), 55 μg/mL catalase (Sigma-Aldrich)), and ultra-centrifugated (278.088 g, 15 min, 4 °C) just before the experiment.

The chamber was sealed and self-organizing microtubule bundles with PRC1 and KIF4A-rich antiparallel overlaps, held close to the glass surface by the depletion force caused by methylcellulose, were imaged at 30 °C on a TIRF microscope.

Reorganization of minimal anaphase midzones by diffusive protein addition from a reservoir

Flow chambers were assembled using one biotin-PEG-functionalized glass and one PLL-PEG passivated counter glass into which a hole of 1 mm diameter had been cut using a laser cutter (Epilog Mini 18) equipped with a 40 Watts laser. The cutting conditions were set to a single cycle at 5000 Hz, 20% power and 40% speed. A reservoir was built on top of the flow chamber by sticking to the cover glass a 2 mm high piece of silicon rubber (Electron Microscopy Sciences, 70338-32) into which a hole of 6 mm diameter had manually punched using a biopsy tool (Harris) so that the hole in the cover glass was roughly in the middle of the reservoir (see the scheme in Fig. 4A).

Solutions were flowed through the flow chamber and the chamber was sealed as described for 'Self-organization of minimal anaphase midzones'. Then 50 μL of the same final solution as in the flow chamber was added to the reservoir and triple-color TIRF microscopy imaging was started. To reorganize the microtubule network, several minutes after imaging started 5 μL of kinase, phosphatase or kinesin was added to the reservoir in order to deliver these proteins to the flow chamber by diffusion. The specific conditions were:

(1) Delayed KIF4A addition to PRC1-bundles (Fig. 6B and C): 20 nM unphosphorylated or CDK1-phosphorylated PRC1-Alexa546 and 18 μM Alexa647-tubulin in the final solution were allowed to organized microtubules without compacted midzones. After ~5 min, 30 nM KIF4A-mGFP was added to the reservoir above the chamber to test to which extent KIF4A can reorganize pre-formed PRC1-microtubule bundles depending on the phosphorylation state of PRC1.

(2) Metaphase-to-anaphase-like midzone bundle reorganization (phosphatase addition, Fig. 4B): 20 nM CDK1-phosphorylated PRC1-Alexa546, 10 nM KIF4A-mGFP, 18 μM Alexa647-tubulin were allowed to organize metaphase-like bundles. After ~5 min, 500 pM lambda protein phosphatase, 500 μM RO-3306 and 1 mM $MnCl_2$ were added to the reservoir to dephosphorylate PRC1 and induce antiparallel overlap compaction.

(3a) Anaphase-to-metaphase-like reorganization (CDK1 addition, Figs. 5A and 6A): 20 nM unphosphorylated PRC1-Alexa546, 10 nM KIF4A-mGFP, 18 μM Alexa647-tubulin in the final solution were first allowed to organize anaphase-like midzone bundles. After ~10 min, 100 nM CDK1 complex was added to the reservoir above the chamber in order to phosphorylate PRC1 and induce the dissolution of the compact antiparallel microtubule overlaps.

(3b) Metaphase-to-anaphase-like reorganization (phosphatase addition, Fig. 6A): 5–10 min after the dissolution of the compact overlaps in 3a, 500 pM lambda protein phosphatase, 500 μM RO-3306 and 1 mM $MnCl_2$ were added to the reservoir (in addition to the already present CDK1 complex) to dephosphorylate PRC1 again and induce compaction of the overlaps.

Tubulin speckle microscopy in minimal midzones

Flow chamber and experimental protocol were the same as described for 'reorganization of minimal anaphase midzones by diffusive protein addition from a reservoir' except the final solution contained 0.9 μM TAMRA-tubulin (final labeling ratio of 0.005), and PRC1-Alexa546 was replaced by non-fluorescent PRC1-SNAP.

TIRF microscopy imaging

Total internal reflection fluorescence (TIRF) microscopy was performed on a custom microscope (Cairn Research, Faversham, UK) based on a Nikon Ti-E frame with a 100 × 1.49 N.A. Nikon objective lens and rotating 360° TIRF illumination (iLas2, Gattaca).

For dual-color time-lapse imaging of PRC1 binding to the overlaps of antiparallel microtubule pairs, Alexa647-microtubules (638 nm laser excitation) and PRC1-Alexa546 (561 nm laser excitation) were recorded non-simultaneously in separate channels using Andor iXon Ultra 888 EMCCD cameras (100 nm pixel size, exposure time of 100 ms, time-lapse interval of 5 sec, 20 min total recording time).

For triple-color time-lapse imaging, Alexa647-microtubules (638 nm excitation) and KIF4A-mGFP ('end tag assay', 'self-organization assay', 'reorganization assay') or PLK1-FAM (PLK1 binding) (488 nm excitation) were recorded simultaneously, while PRC1-SNAP-Alexa546 (561 nm excitation) was recorded separately. For the reorganization assay, the laser power was set to zero during protein addition to the reservoir. Imaging of the self-organization and reorganization experiments ranged from 20 to 40 min.

Quantification of fluorescence intensity in microtubule overlaps

The intensity of PRC1-Alexa546 or PLK1-FAM were quantified using ImageJ along the overlapping region of microtubule pairs. The process involved for each analyzed microtubule pair:

(1) Manually tracing the antiparallel overlap region with a segmented line (1.9 μm width) defining a region of interest (ROI).

(2) Shifting the same segmented line to a region next to the overlap containing no microtubules to obtain the background intensity.

(3) The background-corrected average fluorescence intensity of PRC1-Alexa546 or PLK1-FAM per pixel across the ROI is obtained by subtracting the background from the ROI intensity.

A total of at least 100 μm of antiparallel overlap was measured per condition in at least 3 separate experiments to determine the average

background-corrected fluorescence intensity and standard error. Intensities were plotted as a function of either PRC1 or PLK1 concentration to generate binding curves.

Determination of microtubule growth speeds

The microtubule growth velocity in PRC1/KIF4A end tag experiments was determined from kymographs using ImageJ. The analysis involved:

(1) Kymographs were generated from manually traced regions of interest containing dynamic microtubules in image stacks of time-lapse movies using the Multi Kymograph plugin. The generated kymographs are two-dimensional images with scales of 100 nm/pixel and 5 s/pixel along the horizontal space and vertical time axes.

(2) The microtubule growth velocity was extracted from the slope of the line manually drawn along the growing microtubule plus end position in the kymographs.

Time-lapse images were recorded for a minimum of 20 min in each condition across 3 independent experiment sets. A total of at least 30 microtubules were measured per condition to determine the average and standard error.

Measurement of antiparallel overlap length in reconstituted minimal midzones

The antiparallel overlap length in self-organized minimal midzones was determined using ImageJ. The analysis process consisted of:

(1) Manually tracing the antiparallel overlap region along the length of the microtubule bundles using a segmented line (1.9 µm width) defining the region of interest (ROI).

(2) Adjusting the ROI manually along the growing microtubule bundles across the time sequence.

(3) Generating an intensity profile plot for all ROIs for the PRC1 channel.

(4) The antiparallel overlap length was calculated by extracting the full width half maximum (FWHM) from the intensity profile plot.

At least 8 time points within a 20 min interval of a total of 10 microtubule bundles for every experimental condition were analyzed from 2 independent experiments to calculate the average overlap length and standard deviation.

Computer Simulations

We simulated 1D bundles composed of 4 microtubules, 2 in each orientation, crosslinked by passive PRC1 and active KIF4A using a model that was previously described[38] and implemented with Cytosim, an open source simulation engine based on Brownian dynamics[58]. In brief, a PRC1 dimer is represented by two individual diffusive heads that are connected by a Hookean elastic linker. PRC1 can only crosslink antiparallel microtubules. Each microtubule has its own 1D lattice of binding sites, with one binding site every 8 nm. PRC1 heads can bind to these sites, but exclude each other from binding to the same lattice site. Unlike for the previous model with only 2 microtubules, we used here 4 microtubules arranged symmetrically, creating 4 times more opportunities for crosslinkers to bind in an antiparallel configuration. A KIF4A motor has one motor head and can associate with PRC1, either PRC1 bound to a microtubule or freely diffusing in solution. When bound to a microtubule, KIF4A walks toward the microtubule plus end on a separate lattice without being hindered by PRC1, assuming that KIF4A and PRC1 walk on a different protofilament. In simulation #1, the unbinding rate k_{off} of the PRC1 takes values of 0.1, 0.01, or 0.001/s to explore the behavior of the antiparallel bundle for different PRC1 affinities. In simulation #2, k_{off} is 0.1/s in the metaphase state and 0.001/s in the anaphase state. The microtubule plus end grows with 30 nm/s in the metaphase state and does not grow in the anaphase state. 400 PRC1 and 56 KIF4A molecules are used in all simulations.

Measurement of antiparallel overlap length of computer simulated mini midzones

To calculate the antiparallel overlap length for the computer simulated mini midzones, we estimated PRC1 intensity profiles as would be observed by fluorescence microscopy by summing point spread functions centered at each PRC1 position at a given time point of the simulation. We approximated the point spread function by a Gaussian function, resulting in the total intensity profile expressed as:

$$I(x) = \sum_{i=1}^{n} \exp\left(-\frac{(x - x_i)^2}{2\sigma^2}\right)$$

Here, x_i represents the position of the i-th microtubule-bound PRC1 and σ is the standard deviation of the Gaussian function, which we set at 800 nm. The antiparallel overlap length was then estimated from the full width half maximum of the intensity profile. For each time point, we calculated the mean overlap length and its standard error based on 10 sets of simulations.

Reporting summary

Further information on research design is available in the Nature Portfolio Reporting Summary linked to this article.

Data availability

Source data are provided with this paper. The mass spectrometry proteomics data have been deposited to the ProteomeXchange Consortium via the PRIDE[59] partner repository with the dataset identifier PXD055933. Source data are provided with this paper.

Code availability

The computational model was simulated using Cytosim, publicly available at https://zenodo.org/uploads/13753764.

References

1. Barisic, M., Rajendraprasad, G. & Steblyanko, Y. The metaphase spindle at steady state - mechanism and functions of microtubule poleward flux. *Semin Cell Dev. Biol.* **117**, 99–117 (2021).
2. Vukusic, K. & Tolic, I. M. Anaphase B: long-standing models meet new concepts. *Semin Cell Dev. Biol.* **117**, 127–139 (2021).
3. Lee, K. Y., Davies, T. & Mishima, M. Cytokinesis microtubule organisers at a glance. *J. Cell Sci.* **125**, 3495–3500 (2012).
4. Douglas, M. E. & Mishima, M. Still entangled: assembly of the central spindle by multiple microtubule modulators. *Semin Cell Dev. Biol.* **21**, 899–908 (2010).
5. Glotzer, M. The 3Ms of central spindle assembly: microtubules, motors and MAPs. *Nat. Rev. Mol. Cell Biol.* **10**, 9–20 (2009).
6. Potapova, T. A. et al. The reversibility of mitotic exit in vertebrate cells. *Nature* **440**, 954–958 (2006).
7. Holder, J., Mohammed, S. & Barr, F. A. Ordered dephosphorylation initiated by the selective proteolysis of cyclin B drives mitotic exit. *Elife* **9**, e59885 (2020).
8. Mishima, M. Centralspindlin in Rappaport's cleavage signaling. *Semin Cell Dev. Biol.* **53**, 45–56 (2016).
9. Nunes Bastos, R. et al. Aurora B suppresses microtubule dynamics and limits central spindle size by locally activating KIF4A. *J. Cell Biol.* **202**, 605–621 (2013).
10. Serena, M., Bastos, R. N., Elliott, P. R. & Barr, F. A. Molecular basis of MKLP2-dependent Aurora B transport from chromatin to the anaphase central spindle. *J. Cell Biol.* **219**, e201910059 (2020).
11. Jiang, W. et al. PRC1: a human mitotic spindle-associated CDK substrate protein required for cytokinesis. *Mol. Cell* **2**, 877–885 (1998).
12. Kurasawa, Y., Earnshaw, W. C., Mochizuki, Y., Dohmae, N. & Todokoro, K. Essential roles of KIF4 and its binding partner PRC1 in

organized central spindle midzone formation. *EMBO J.* **23**, 3237–3248 (2004).
13. Mollinari, C. et al. PRC1 is a microtubule binding and bundling protein essential to maintain the mitotic spindle midzone. *J. Cell Biol.* **157**, 1175–1186 (2002).
14. Zhu, C. & Jiang, W. Cell cycle-dependent translocation of PRC1 on the spindle by Kif4 is essential for midzone formation and cytokinesis. *Proc. Natl Acad. Sci. USA* **102**, 343–348 (2005).
15. Asthana, J., Cade, N. I., Normanno, D., Lim, W. M. & Surrey, T. Gradual compaction of the central spindle decreases its dynamicity in PRC1 and EB1 gene-edited cells. *Life Sci. Alliance* **4**, e202101222 (2021).
16. Kajtez, J. et al. Overlap microtubules link sister k-fibres and balance the forces on bi-oriented kinetochores. *Nat. Commun.* **7**, 10298 (2016).
17. Khmelinskii, A., Roostalu, J., Roque, H., Antony, C. & Schiebel, E. Phosphorylation-dependent protein interactions at the spindle midzone mediate cell cycle regulation of spindle elongation. *Dev. Cell* **17**, 244–256 (2009).
18. Loiodice, I. et al. Ase1p organizes antiparallel microtubule arrays during interphase and mitosis in fission yeast. *Mol. Biol. Cell* **16**, 1756–1768 (2005).
19. Pamula, M. C. et al. High-resolution imaging reveals how the spindle midzone impacts chromosome movement. *J. Cell Biol.* **218**, 2529–2544 (2019).
20. Gluszek-Kustusz, A., Craske, B., Legal, T., McHugh, T. & Welburn, J. P. Phosphorylation controls spatial and temporal activities of motor-PRC1 complexes to complete mitosis. *EMBO J.* **42**, e113647 (2023).
21. Lee, K. Y., Esmaeili, B., Zealley, B. & Mishima, M. Direct interaction between centralspindlin and PRC1 reinforces mechanical resilience of the central spindle. *Nat. Commun.* **6**, 7290 (2015).
22. Lee, Y. M. & Kim, W. Kinesin superfamily protein member 4 (KIF4) is localized to midzone and midbody in dividing cells. *Exp. Mol. Med* **36**, 93–97 (2004).
23. Bieling, P., Telley, I. A. & Surrey, T. A minimal midzone protein module controls formation and length of antiparallel microtubule overlaps. *Cell* **142**, 420–432 (2010).
24. Janson, M. E. et al. Crosslinkers and motors organize dynamic microtubules to form stable bipolar arrays in fission yeast. *Cell* **128**, 357–368 (2007).
25. Subramanian, R. et al. Insights into antiparallel microtubule crosslinking by PRC1, a conserved nonmotor microtubule binding protein. *Cell* **142**, 433–443 (2010).
26. Malik, R. et al. Quantitative analysis of the human spindle phosphoproteome at distinct mitotic stages. *J. Proteome Res* **8**, 4553–4563 (2009).
27. Neef, R. et al. Choice of Plk1 docking partners during mitosis and cytokinesis is controlled by the activation state of Cdk1. *Nat. Cell Biol.* **9**, 436–444 (2007).
28. Cundell, M. J. et al. The BEG (PP2A-B55/ENSA/Greatwall) pathway ensures cytokinesis follows chromosome separation. *Mol. Cell* **52**, 393–405 (2013).
29. do Rosario, C. F., Zhang, Y., Stadnicki, J., Ross, J. L. & Wadsworth, P. Lateral and longitudinal compaction of PRC1 overlap zones drives stabilization of interzonal microtubules. *Mol. Biol. Cell* **34**, ar100 (2023).
30. Hu, C. K., Ozlu, N., Coughlin, M., Steen, J. J. & Mitchison, T. J. Plk1 negatively regulates PRC1 to prevent premature midzone formation before cytokinesis. *Mol. Biol. Cell* **23**, 2702–11 (2012).
31. Subramanian, R., Ti, S. C., Tan, L., Darst, S. A. & Kapoor, T. M. Marking and measuring single microtubules by PRC1 and kinesin-4. *Cell* **154**, 377–390 (2013).
32. Bringmann, H. et al. A kinesin-like motor inhibits microtubule dynamic instability. *Science* **303**, 1519–1522 (2004).
33. Hu, C. K., Coughlin, M., Field, C. M. & Mitchison, T. J. KIF4 regulates midzone length during cytokinesis. *Curr. Biol.* **21**, 815–824 (2011).
34. Nedelec, F. J., Surrey, T., Maggs, A. C. & Leibler, S. Self-organization of microtubules and motors. *Nature* **389**, 305–308 (1997).
35. Surrey, T., Nedelec, F., Leibler, S. & Karsenti, E. Physical properties determining self-organization of motors and microtubules. *Science* **292**, 1167–1171 (2001).
36. Roostalu, J., Rickman, J., Thomas, C., Nedelec, F. & Surrey, T. Determinants of polar versus nematic organization in networks of dynamic microtubules and mitotic motors. *Cell* **175**, 796–808 e714 (2018).
37. Sanchez, T., Chen, D. T., DeCamp, S. J., Heymann, M. & Dogic, Z. Spontaneous motion in hierarchically assembled active matter. *Nature* **491**, 431–434 (2012).
38. Hannabuss, J. et al. Self-organization of minimal anaphase spindle midzone bundles. *Curr. Biol.* **29**, 2120–2130.e2127 (2019).
39. Wijeratne, S. & Subramanian, R. Geometry of antiparallel microtubule bundles regulates relative sliding and stalling by PRC1 and Kif4A. *Elife* **7**, e32595 (2018).
40. Mani, N., Jiang, S., Neary, A. E., Wijeratne, S. S. & Subramanian, R. Differential regulation of single microtubules and bundles by a three-protein module. *Nat. Chem. Biol.* **17**, 964–974 (2021).
41. Huis In, t Veld, P. J. et al. Reconstitution and use of highly active human CDK1:Cyclin-B:CKS1 complexes. *Protein Sci.* **31**, 528–537 (2022).
42. Singh, P. et al. BUB1 and CENP-U, primed by CDK1, are the main PLK1 kinetochore receptors in mitosis. *Mol. Cell* **81**, 67–87.e69 (2021).
43. Adriaans, I. E., Basant, A., Ponsioen, B., Glotzer, M. & Lens, S. M. A. PLK1 plays dual roles in centralspindlin regulation during cytokinesis. *J. Cell Biol.* **218**, 1250–1264 (2019).
44. Cundell, M. J. et al. A PP2A-B55 recognition signal controls substrate dephosphorylation kinetics during mitotic exit. *J. Cell Biol.* **214**, 539–554 (2016).
45. Lemma, B., Mitchell, N. P., Subramanian, R., Needleman, D. J. & Dogic, Z. Active microphase separation in mixtures of microtubules and tip-accumulating molecular motors. *Phys. Rev. X* **12**, 031006 (2022).
46. Sahu, S. et al. Interplay of self-organization of microtubule asters and crosslinking protein condensates. *PNAS Nexus* **2**, pgad231 (2023).
47. Petronczki, M., Glotzer, M., Kraut, N. & Peters, J. M. Polo-like kinase 1 triggers the initiation of cytokinesis in human cells by promoting recruitment of the RhoGEF Ect2 to the central spindle. *Dev. Cell* **12**, 713–725 (2007).
48. Chandrakar, P. et al. Engineering stability, longevity, and miscibility of microtubule-based active fluids. *Soft Matter* **18**, 1825–1835 (2022).
49. Braun, M. et al. Adaptive braking by Ase1 prevents overlapping microtubules from sliding completely apart. *Nat. Cell Biol.* **13**, 1259–1264 (2011).
50. Poser, E., Caous, R., Gruneberg, U. & Barr, F. A. Aurora a promotes chromosome congression by activating the condensin-dependent pool of KIF4A. *J. Cell Biol.* **219**, e201905194 (2019).
51. Takata, H., Madung, M., Katoh, K. & Fukui, K. Cdk1-dependent phosphorylation of KIF4A at S1186 triggers lateral chromosome compaction during early mitosis. *PLoS One* **13**, e0209614 (2018).
52. Trowitzsch, S., Bieniossek, C., Nie, Y., Garzoni, F. & Berger, I. New baculovirus expression tools for recombinant protein complex production. *J. Struct. Biol.* **172**, 45–54 (2010).
53. Hashimoto, Y., Zhang, S., Zhang, S., Chen, Y. R. & Blissard, G. W. Correction: BTI-Tnao38, a new cell line derived from Trichoplusia ni, is permissive for AcMNPV infection and produces high levels of recombinant proteins. *BMC Biotechnol.* **12**, 12 (2012).
54. Castoldi, M. & Popov, A. V. Purification of brain tubulin through two cycles of polymerization-depolymerization in a high-molarity buffer. *Protein Expr. Purif.* **32**, 83–88 (2003).
55. Consolati, T., Henkin, G., Roostalu, J. & Surrey, T. Real-time imaging of single gammaTuRC-mediated microtubule nucleation events

in vitro by TIRF microscopy. *Methods Mol. Biol.* **2430**, 315–336 (2022).
56. Jeong, H. J., Abhiraman, G. C., Story, C. M., Ingram, J. R. & Dougan, S. K. Generation of Ca2+-independent sortase A mutants with enhanced activity for protein and cell surface labeling. *PLoS One* **12**, e0189068 (2017).
57. Olivella, R. et al. QCloud2: an improved cloud-based quality-control system for mass-spectrometry-based proteomics laboratories. *J. Proteome Res* **20**, 2010–2013 (2021).
58. Nedelec, F. & Foethke, D. Collective Langevin dynamics of flexible cytoskeletal fibers. *N. J. Phys.* **9**, 427 (2007).
59. Perez-Riverol, Y. et al. The PRIDE database resources in 2022: a hub for mass spectrometry-based proteomics evidences. *Nucleic Acids Res* **50**, D543–D552 (2022).

Acknowledgements

We thank the CRG/UPF Proteomics Unit, which is part of the Spanish Infrastructure for Omics Technologies (ICTS OmicsTech), for performing the proteomics analysis, Martina Trokter for cloning the GFP expression construct, Silvia Speroni for purifying GFP, Kseniya Ustinova for preparing TAMRA-labeled tubulin, Julian Gannon, Maria Gili and Raquel Garcia-Castellanos for protein expression and purification support, Felix Ruhnow for microscopy support and for help with developing the flow chamber with the top reservoir, Roberto Paoli for microfabrication support at the μFabLab at the Barcelona Biomedical Research Park (PRBB), François Nédélec for advice regarding the computer simulations, and Zoë Geraghty and Philippe Cluzel for useful discussions. We acknowledge support of the Spanish Ministry of Science and Innovation through the Centro de Excelencia Severo Ochoa (CEX2020-001049-S, MCIN/AEI /10.13039/501100011033), and the Generalitat de Catalunya through the CERCA program. We are grateful to the CRG Core Technologies Program for their support and assistance.This project has received funding from the European Research Council (ERC) under the European Union's Horizon 2020 research and innovation program (grant agreement No 951430; T.S. and A.M.) and received support from the Spanish Ministry of Science and Innovation (grants PID2019-108415GB-I00 / AEI / 10.13039/501100011033 and PID2022-142927NB-I00 / AEI / 10.13039/501100011033; T.S.). W.-X.C. was supported by a Human Frontier Science Program fellowship (HFSP LT000682/2020-C).

Author contributions

W.M.L. generated expression constructs, expressed and purified cytoskeletal proteins, conceived and performed phosphorylation and microscopy experiments, and analyzed data. W.-X.C. performed computer simulations and analyzed data. A.E.V. and M.P. generated expression constructs, expressed and purified kinases and phosphatases, and provided technical expertize. T.S. and W.M.L. wrote the original draft. All authors contributed to writing the manuscript. T.S. and A.M. supervised the project and secured funding.

Competing interests

The authors declare no competing interests.

Additional information

Supplementary information The online version contains supplementary material available at https://doi.org/10.1038/s41467-024-53500-1.

Correspondence and requests for materials should be addressed to Thomas Surrey.

Peer review information *Nature Communications* thanks Francis Barr, and the other, anonymous, reviewer(s) for their contribution to the peer review of this work. A peer review file is available.